MODELING AND EXPERIMENTAL STUDIES OF PC/ABS AT LARGE DEFORMATIONS

Master's Dissertation by

Henrik Persson and Kent Ådán

Supervisors
Vijay Sharan, Sony Ericsson
Mathias Wallin, Div. of Solid Mechanics
Paul Håkansson, Div. of Solid Mechanics
Matti Ristinmaa, Div. of Solid Mechanics

Preface

This Master's Thesis was done at the request of Sony Ericsson Mobile Communications AB and with supervision from the Division of Solid Mechanics, Lund University during the period of September 2003 to March 2004. The primary work has been done at Sony Ericsson Mobile in Lund. The material tests and computer simulations have been made at the University of Lund.

The thesis was carried out in order to adapt an existing material model in ANSYS that describe one of the thermoplastic materials that Sony Ericsson currently uses. During this period of time we have learned a lot about practical tests combined with advanced theoretical studies of material behaviour. The many issues we have faced have given many new aspects of the problems that an engineer deals with.

Lund, March 2004

Henrik Persson, Kent Ådán

Abstract

This Master's Thesis was done in collaboration with the division of solid Mechanics at University of Lund and Sony Ericsson Mobile Communications AB. The objective for the assignment was to adopt a material model that describes one of the thermoplastic materials that Sony Ericsson currently uses. This was done to, in a more accurate way than present, anticipate fault in the construction before starting the manufacturing process. In this Master's Thesis, different kinds of rate-dependent constitutive models were investigated. The purpose was to find out what properties that can be simulated and what cannot. The focus of the investigation of material models was towards models that are implemented in ANSYS.

After a strictly theoretical examine of suitable material models, tensile tests were performed in order to understand the qualitative behaviour of the thermoplastic material. Constant displacement rate tension tests were performed on all test specimens for comparison with the simulated tensile test results from finite element analysis. A displacement controlled application was chosen because of the critical necking phase. Due to the lack of test equipment that could measure the cross section area decrease, we had to find this area dependent stress-strain data by comparing simulated data with data from tensile tests.

There are only two material models available in ANSYS that are suitable for modelling large strain rate-dependent plasticity, namely the *Perzyna* model or the *Peirce* model. Both of the models must be used in combination with isotropic hardening plasticity. The isotropic hardening plasticity is described by an input of a true stress-strain curve. Peirce model did not describe the thermoplastic material in a satisfying manner, hence this model was excluded.

There are very limited ways of calibrating the constitutive models in ANSYS. To simulate the viscous behaviour of the investigated thermoplastic, the viscosity parameters must be adapted in the Perzyna model. All made tensile tests at the different strain rates were simulated in ANSYS with the selected parameters, until satisfying results were achieved.

The Perzyna model describes the mechanical behaviour well, for the investigated strain rates. The overall test results show satisfactory agreement with the simulated results, with the only exception for static condition where the agreement between real tests and simulations were not totally satisfying in the softening region. This is due to the limitations in the plastic material model.

Tensile tests, with ordinary test specimens are suitable for analyzing material behaviour. Unfortunately this test technique can only describe material behaviour in one dimension. Therefore a verification test was needed, that could describe the whole stress field. This test was made in the same way as an ordinary tensile test process, but with a slightly modified test specimen. The simulated results showed a high agreement with the tensile test results. This is a proof of that the Perzyna model can describe more complicated geometries at a higher strain rate for the investigated PC/ABS plastic, more accurately, than with the presently used material model.

Contents

1 Introduction

1.1 Presentation of Sony Ericsson Mobile Communications AB

In 2001 the company Sony Ericsson Mobile Communications AB was established by telecommunications leader Ericsson and Sony Corporation. The company is equally owned by Ericsson and Sony.

Sony Ericsson is responsible for product research, development and design, as well as marketing and sales, distribution and customer's service. The company's global corporate management is based in London. Approximately 3,500 employees are working around the world. The company's President is Katsumi Ihara, and Executive Vice President is Jan Wäreby.

The new company's first joint product was announced in March 2002 and now has a complete portfolio covering all target groups. The combine strength of Sony and Ericsson, and its strong consumer-focused and application-led strategy, make the company a leading player in the mobile communications industry [21].

1.2 Background to the assignment

The cellular telephone market is in an expanding phase. Nowadays consumers use the phone in many different environments and in a reckless way, influencing the demands on strength of the phone. Without taking this into account before the production, this may cause great expenditure and negatively impact the company's reputation. Currently, a diverse collection of plastic materials are widely used for reduction of weight and manufacturing costs.
By using FE calculations to predict the characteristics of the phone in an early phase many expensive errors can be avoided. Today there is no accurate material model used at Sony Ericsson that supports simulations of thermoplastic materials exposed to large deformations. The background for the assignment is therefore to investigate and find the most suitable constitutive model implemented in ANSYS that supports large deformation, for the thermoplastic material Sony Ericsson presently uses.

1.3 Objectives

In this Master's Thesis, different kinds of constitutive models for thermoplastic materials were investigated. Currently Sony Ericsson uses a material model that is not satisfying regarding high strain rate applications. The objective of the project was to determine the properties of the thermoplastic materials, by performing material testing. The experimental results were adapted to an existing material model in ANSYS, with restrictions taking into account. The FE-simulations of a test specimen were compared with the result from real tensile tests.

1.4 Restrictions

The analysis does not accommodate material characteristics pertaining to the thermal behaviour of the materials or effects of creep. Short term time dependent properties of the specified thermoplastic material, were however considered for the adoption. There are a few material models available in ANSYS that may be suited for the specified thermoplastic. Unfortunately, the limited time in a Master's Thesis does not allow implementing own derived models.

In this thesis the structure of the thermoplastic material is assumed to be isotropic before and after the material has been deformed, which may affect the accuracy of the result.

Some parts in this thesis have been omitted due to the request for secrecy; this explains the normalized values on the axes for all represented graphs, throughout this work.

2 Presentation of thermoplastic materials

2.1 History

The material in its natural manner has been known in China and Egypt for many thousand years. Still, this material should be taken as new and undeveloped in many aspects. As early as in the 19th century, the chemists learned how to make use of natural macro molecules and ennoble them into half synthetics plastics. The discovery of cellulose nitrate, in the 1860 was a breakthrough for the plastics [15].

In the beginning of 20th century L Baekeland discovered phenol and formaldehyde (Bakelite). After that followed, from the middle of 1920 polyester plastic and polystyrene, among others were discovered [15].

In the 1930s, there was an intensive research on polymers, mainly in Germany and USA. Following this successful research, acrylic plastic (Plexiglas) and polyamide (Nylon) made their entrance. Nylon made a breakthrough during the Second World War, when it replaced the more expensive silk parachutes [7].

In modern time, the development of plastic materials is undergoing rapid progress and new materials are continually introduced. The reason why plastics have been so widely used mainly depends on its low weight and low manufacturing costs.

2.2 The characteristics of the plastics

Traditionally, plastics are divided into thermoplastics and thermosets. In the thermosets, molecule chains are transversally linked into a three dimensional network. The hardening process starts first after a heat treatment or after adding a setting agent. The hardening process is not reversible and the plastic is therefore not recyclable, as the thermoplastics are. Thermoplastics, on the other hand, consist of long chains of monomers from the polymerization process. The common machining capability for this plastic is injection molding and extrusion.

Both of the plastics mentioned above, are suitable for addition of filling material, which change the properties of the material radically. The addition substance can be pigment, elasticizer, armoring, external flame retardant among others.

One of the thermoplastic materials that Sony Ericsson is currently using is PC/ABS, an amorphous polycarbonate and acrylonitrile-butadiene-styrene thermoplastic polymer blend. PC/ABS has many manufacturing advantages when it comes to injection molding and extrusion. It has excellent filling capability for long and complex parts, without influencing the mechanical properties significantly. The plastic has excellent ductility, also at sub zero temperatures and it has a good heat resistance. Other engineering features of PC/ABS are the impact toughness and the relative rigidity it gives the product [10]. Sony Ericsson mostly uses PC/ABS for the shell of cellular telephones. The shell among other parts of the cellular telephone is produced by injection molding.

3 Introduction to large deformations

When the strain exceeds more than a few percent a theory for large strain and large rotation must be used, since the geometry has deformed to an extent where the geometry change can not be neglected.

Many applications of thermoplastic materials are subjected to deformations that can not be approximated as small. To describe thermoplastic materials when subjected to large strain or/and large rotations, more advanced theory needs to be considered [3]. Tensor notation is often used in tensor algebra to rewrite complicated expressions in a very compact fashion. Throughout this Master's Thesis only Cartesian tensors will be considered.

3.1 An introduction to Cartesian index notation and tensor algebra

To more easily understand the mathematical expression used in this master thesis, an introduction of tensor algebra will follow. The described theory in chapter 3.1 is taken from [19], if nothing else is indicated.

A first order tensor a_i can be rewritten into a column matrix and be expressed as

$$[a_i] = \begin{bmatrix} a_1 \\ a_2 \\ a_3 \end{bmatrix}, \quad where \quad i = 1, 2 \text{ or } 3 \tag{3.1}$$

In what follows, Latin indices, unless otherwise specified, assume the values 1, 2 or 3. There are some conventions in index notation that will be mentioned below.

If the same index is repeated twice, it is called a *dummy* index and otherwise it is called a *free* index. An example of the *summation convention* is the product $a_i b_i$

$$a_i b_i = a_1 b_1 + a_2 b_2 + a_3 b_3 \tag{3.2}$$

It should be pointed out that the same index can appear not more than twice, otherwise the choice of index has no influence.

The second order tensor B_{ij} can be expressed in matrix format as

$$[B_{ij}] = \begin{bmatrix} B_{11} & B_{12} & B_{13} \\ B_{21} & B_{22} & B_{23} \\ B_{31} & B_{32} & B_{33} \end{bmatrix} \tag{3.3}$$

Kronecker delta δ_{ij} which plays an essential role in index notation and tensor algebra is defined as

$$\delta_{ij} = \begin{cases} 1 & if \ i = j \\ 0 & if \ i \neq j \end{cases} \tag{3.4}$$

Using the Kronecker delta and the summation convention the following can now be expressed

$$B_{ij}\delta_{jk} = B_{ik} \qquad (3.5)$$

Tensors must behave in a certain manner when exposed of translations and rotations. The different grades of tensors used in this thesis, are defined as

$$b = b' \quad \textit{zero order tensor} \qquad (3.6)$$

$$x_i = A_{ji}x'_j \quad \textit{first order tensor} \qquad (3.7)$$

$$T_{ij} = A_{li}T'_{lk}A_{kj} \quad \textit{second order tensor} \qquad (3.8)$$

3.2 Description of motion of deformation

3.2.1 Deformation gradient

The expressions in chapter 3.2, are if not stated otherwise, taken from [18]. The loads acting on a body, makes it move from one position to another. This motion can be defined by studying a position vector in the deformed and undeformed configuration. At time $t = 0$, before any motion, the position vector of a particle is described by the coordinates X_i in the undeformed configuration. The position of the particle in the deformed configuration at time t is described by the position vector x_i, see Figure 3.1.
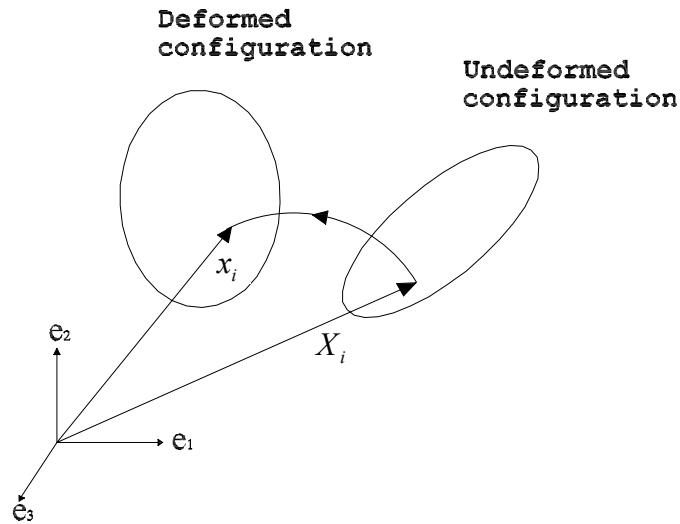

Figure 3.1: The undeformed and deformed configuration.

The *material deformation gradient* maps a material point from the undeformed configuration into the deformed configuration and can be expressed as [16]

$$F_{ij} = \frac{\partial x_i}{\partial X_j} \qquad (3.9)$$

A conversion between dX_j and dx_i can now easily be made

$$dx_i = F_{ij}dX_j \quad or \quad dX_i = F_{ij}^{-1}dx_j \qquad (3.10)$$

which describes how the relative position vector dX_j in the undeformed configuration has transformed to the position vector dx_i in the deformed configuration.

The deformation gradient F_{ij} contains information of the volume change, the rotation and the shape change of the deformed body. The volume change can be expressed as

$$J = \frac{dV}{dV_0} = \det F_{ij} \qquad (3.11)$$

where V_0 is the original volume in the undeformed configuration and V is the current volume in the deformed configuration. The determinant J of the second order tensor F_{ij} is called the Jacobian.

The determinant of the tensor is an invariant, i.e. independent of the chosen coordinate system. If $J = 1$ for all X_i, the volume of the deformed and undeformed configuration are identical and the deformation is said to be isochoric.

3.2.2 Strain tensors

To describe the motion of the body in more detail, it is of interest to obtain quantities that only depend on the deformation of the body and not the rigid body motion; such quantities are called strain tensors.

The deformation of a body is related to the change of distance between some particles. Due to motion of the body the vector dX_i, between two closely spaced particles in the undeformed configuration, changes into the vector dx_i between the same particles, see Figure 3.2.
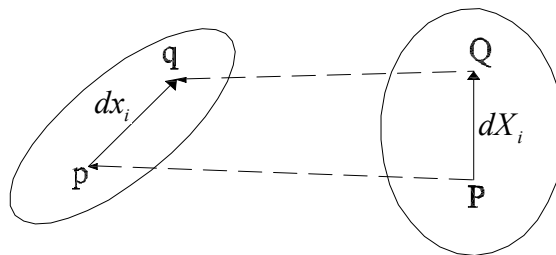

Figure 3.2: Points P and p refer to the same particle; points Q and q refer to the same particle.

The length of vector dX_i is denoted by dS and the length of vector dx_i is denoted by ds. These two measures tell something about the deformation of the body; rigid body motion means that $ds = dS$ i.e.

6

$$dS^2 = dX_i dX_i; \qquad ds^2 = dx_i dx_i \tag{3.12}$$

According to (3.10a), it follows that

$$ds^2 = dX_j C_{jk} dX_k \tag{3.13}$$

where

$$C_{jk} = \frac{\partial x_i}{\partial X_j} \frac{\partial x_i}{\partial X_k} = F_{ij} F_{ik} \tag{3.14}$$

The tensor C_{ij} is termed the *right Cauchy-Green deformation tensor* and, moreover, it is noted that it is symmetric, i.e. $C_{jk} = C_{kj}$.

A comparison of the lengths ds and dS is interesting in order to characterize the deformation, with (3.12) and (3.13) it follows that

$$ds^2 - dS^2 = 2 dX_i E_{ij} dX_j \tag{3.15}$$

where

$$E_{ij} = \frac{1}{2}(C_{ij} - \delta_{ij}) = \frac{1}{2}\left(F_{ki} F_{kj} - \delta_{ij}\right) = \frac{1}{2}\left(\frac{\partial x_k}{\partial X_i} \frac{\partial x_k}{\partial X_j} - \delta_{ij}\right) \tag{3.16}$$

is termed the *Lagrangian strain tensor.*

In (3.16), the derivatives are taken with respect to X_i, but it is also possible to obtain an expression for $ds^2 - dS^2$, which involves derivatives with respect to x_i. Insertion of (3.10b) into (3.12a) yields

$$dS^2 = dx_j c_{jk} dx_k \tag{3.17}$$

where

$$c_{jk} = \frac{\partial X_i}{\partial x_j} \frac{\partial X_i}{\partial x_k} \tag{3.18}$$

is termed *Cauchy's deformation tensor*.

The *left Cauchy-Green deformation tensor* is introduced as

$$b_{ij} = c_{ij}^{-1} = F_{ik} F_{jk} \tag{3.19}$$

3.2.3 Stretch tensors

Another measurement of deformation of a body is the elongation or shortening of the distance between two close particles. Such a measure is provided by the so-called stretch.

$$\Lambda = \frac{ds}{dS} \tag{3.20}$$

where dS and ds have been defined earlier.

To relate the stretch to the different deformation measures, the unit vector $\overline{N}_i$, in the direction of dX_i is introduced

$$\overline{N}_i = \frac{dX_i}{dS} \tag{3.21}$$

From (3.13), (3.20) and (3.21) it appears that

$$\Lambda^2 = \overline{N}_i C_{ij} \overline{N}_j \tag{3.22}$$

As seen in (3.22) the right Cauchy-Green deformation tensor is related to the square of the stretch Λ, therefore it is of interest to seek a deformation tensor which is linear in the stretch. Therefore the following expression is introduced

$$U_{ij} = \sqrt{C_{ij}} \tag{3.23}$$

This tensor U_{ij} is named the *right stretch tensor*.

In the same manner using the left Cauchy-Green deformation tensor an analogous *left stretch tensor* can be defined as

$$V_{ij} = \sqrt{b_{ij}} \tag{3.24}$$

The *polar decomposition theorem* of Cauchy will be used below. It states that there exists two unique symmetric positive definite tensors U_{ij} and V_{ij}, the right and left stretch tensor, and an orthogonal tensor R_{ij} such that

$$F_{ij} = R_{ik} U_{kj} \quad or \quad F_{ij} = V_{ik} R_{kj} \tag{3.25}$$

where R_{ij} is the rotation tensor.

8

3.3 Rate of deformation tensor

From (3.16) the Lagrangian strain tensor E_{ij} is introduced and it has been shown that this tensor provides a complete description of the deformation of the body using the material description, independent of rigid body motions.

In some cases it is not the total change of deformation that is of importance, but rather the time rate with which these changes occur. When the constitutive equations are formulated in rate form like elasto-plasticity this situation arises. Therefore it is necessary to establish a tensor, which describes the rate with which deformation occurs. The theory throughout chapter 3.3 is taken from [18], if nothing else is indicated.

Once again consider the length ds of the vector dx_i connecting two neighbouring particles in the deformed configuration, see Figure 3.2. This length is given by (3.12b). The material derivative of this expression gives

$$ds \frac{D(ds)}{Dt} = dx_i \frac{D(dx_i)}{Dt}$$

(3.26)

If F_{ij} is expressed in material coordinates, i.e. $F_{ij} = F_{ij}(X_k,t)$, the material derivative of (3.10a) then gives

$$\frac{D(dx_i)}{Dt} = \frac{DF_{ij}}{Dt} dX_j + F_{ij} \frac{D(dX_j)}{Dt}$$

(3.27)

The vector dX_j is independent of time, so the expression above can be reduced to

$$\frac{D(dx_i)}{Dt} = \frac{DF_{ij}}{Dt} dX_j$$

(3.28)

To evaluate the term DF_{ij}/Dt, the material coordinates are adopted and it follows that

$$\frac{DF_{ij}}{Dt} = \frac{\partial F_{ij}}{\partial t} = \frac{\partial}{\partial t}\left(\frac{\partial x_i(X_k,t)}{\partial X_j} \right) = \frac{\partial}{\partial X_j}\left(\frac{\partial x_i(X_k,t)}{\partial t} \right) = \frac{\partial v_i}{\partial X_j}$$

(3.29)

where (3.26) was used. This implies that (3.28) can be rewritten as

$$\frac{D(dx_i)}{Dt} = \frac{\partial v_i}{\partial X_j} dX_j$$

(3.30)

If the velocity is expressed in terms of Eulerian coordinates, i.e. $v_i = v_i(x_k,t)$, it follows that

$$\frac{\partial v_i}{\partial X_j} = \frac{\partial v_i}{\partial x_k} \frac{\partial x_k}{\partial X_j} = \frac{\partial v_i}{\partial x_k} F_{kj}$$

(3.31)

(3.30) then takes the form

$$\frac{D(dx_i)}{Dt} = \frac{\partial v_i}{\partial x_k} F_{kj} dX_j \tag{3.32}$$

which with (3.10a) becomes

$$\frac{D(dx_i)}{Dt} = \frac{\partial v_i}{\partial x_k} dx_k \tag{3.33}$$

The *spatial velocity gradient* L_{ij} is defined by

$$L_{ij} = \frac{\partial v_i}{\partial x_j} \tag{3.34}$$

Then (3.33) can be written as

$$\frac{D(dx_i)}{Dt} = L_{ij} dx_j \tag{3.35}$$

By introducing (3.35) into (3.26), it follows that

$$ds \frac{D(ds)}{Dt} = dx_i L_{ij} dx_j \tag{3.36}$$

The unit vector in direction dx_i is given by $n_i = dx_i / ds$, which allows (3.36) to be written as

$$\frac{1}{ds} \frac{D(ds)}{Dt} = n_i L_{ij} n_j \tag{3.37}$$

To rewrite this expression recall (3.20). It follows that

$$\frac{D(ds)}{Dt} = \frac{D\Lambda}{Dt} dS = \frac{D\Lambda}{Dt} \frac{ds}{\Lambda} \tag{3.38}$$

Insertion into (3.37) gives

$$\frac{1}{\Lambda} \frac{D\Lambda}{Dt} = n_i L_{ij} n_j \tag{3.39}$$

It appears that the material derivative of the stretch in the direction given by the unit vector n_i in the deformed configuration is related to the spatial velocity gradient L_{ij}.

10

It is always possible to split L_{ij} into a symmetric part D_{ij} and an unsymmetrical part W_{ij} according to

$$L_{ij} = D_{ij} + W_{ij} \tag{3.40}$$

where

$$D_{ij} = \frac{1}{2}\left(\frac{\partial v_i}{\partial x_j} + \frac{\partial v_j}{\partial x_i}\right) \quad \textit{rate of deformation tensor} \tag{3.41}$$

and

$$W_{ij} = \frac{1}{2}\left(\frac{\partial v_i}{\partial x_j} - \frac{\partial v_j}{\partial x_i}\right) \quad \textit{spin tensor} \tag{3.42}$$

Now it is possible to establish the relation between the rate of deformation tensor D_{ij} and the material derivative $\dot{E}_{ij}$ of the Lagrangian strain. Next, (3.16) gives

$$\dot{E}_{ij} = \frac{1}{2}\left(\dot{F}_{ki}F_{kj} + F_{ki}\dot{F}_{kj}\right) \tag{3.43}$$

In order to determine the quantity $\dot{F}_{kj}$, (3.29), (3.31) and (3.34) are used to give

$$\dot{F}_{ij} = \frac{\partial v_i}{\partial X_j} = \frac{\partial v_i}{\partial x_k}F_{kj} = L_{ik}F_{kj} \tag{3.44}$$

This expression together with (3.43) and (3.40) gives the sought relation

$$\dot{E}_{ij} = F_{ik}D_{kl}F_{lj} \tag{3.45}$$

3.4 Stress tensors

The expressions in this section are if not stated otherwise, taken from [18]. To establish the equations of motion, consider a body in its deformed configuration and make a section throughout the particle P. The normal n_i to the section is directed outwards of the body, cf. Figure 3.3.
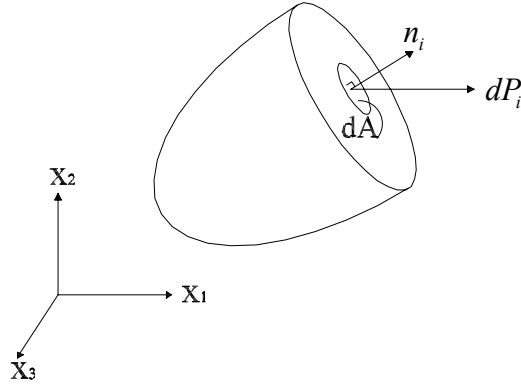

Figure 3.3: Force dP$_i$ and area dA with outer unit normal vector n$_i$.

On the incremental area dA surrounding the particle, the incremental force dP_i acts and the traction tensor t_i is then defined as

$$t_i = \frac{dP_i}{dA} \tag{3.46}$$

If another section trough the same particle is taken, a different traction tensor will in general be obtained. Therefore, the traction tensor is a function of the direction n_j, i.e.

$$t_i = t_i(n_j) \tag{3.47}$$

If a direction parallel with one of the x_i-axis is chosen, a certain traction t_i tensor is obtained. Consequently there exists three certain traction tensors, one for each x_i-axis. This traction tensor can be expressed as

$$[t_i] = \begin{bmatrix} \sigma_{i1} \\ \sigma_{i2} \\ \sigma_{i3} \end{bmatrix} \tag{3.48}$$

There are several different stress tensors. The stress tensor, which represents the true stress, is called Cauchy stress tensor σ_{ij} and is defined as

$$[\sigma_{ij}] = \begin{bmatrix} t_1^T \\ t_2^T \\ t_3^T \end{bmatrix} = \begin{bmatrix} \sigma_{11} & \sigma_{12} & \sigma_{13} \\ \sigma_{21} & \sigma_{22} & \sigma_{23} \\ \sigma_{31} & \sigma_{32} & \sigma_{33} \end{bmatrix} \tag{3.49}$$

12

Two other stress tensors was introduced by Piola in 1833 and by Kirchhoff in 1852, where the first Piola-Kirchhoff stress tensor is defined as

$$P_{ij} = J\sigma_{ik}\frac{\partial X_j}{\partial x_k}$$

(3.50)

and the second Piola-Kirchhoff stress is defined as

$$S_{kl} = J\frac{\partial X_k}{\partial x_i}\sigma_{ij}\frac{\partial X_l}{\partial x_j}$$

(3.51)

The first Piola-Kirchhoff tensor is unsymmetric and the second Piola-Kirchhoff tensor is symmetric.

Another stress tensor is the Kirchhoff's stress tensor which is defined as

$$\tau_{ij} = J\sigma_{ij}$$

(3.52)

4 Constitutive models

4.1 Material frame indifference

One of the requirements of the constitutive relations are that they must be coordinate invariant, i.e. if a constitutive relation holds in one coordinate system, it must hold in any other coordinate system. This requirement is fulfilled, when the constitutive relation is formulated in tensor quantities.

Unfortunately the coordinate invariance is not enough, since it is also possible to change frame. Therefore the principle of frame indifference must be fulfilled as well, i.e. a function valid in one frame must be valid in all frames.

In constitutive modelling and especially within plasticity theory, an introduction of the time-rate of the stress tensor is of interest. It is often found that the material derivate of an objective stress tensor is not always objective. An objective tensor must transform in a similar manner when the frame is changed as when the coordinate system is changed. To demonstrate this, the objective Cauchy stress tensor will be investigated

$$\sigma_{ij} = Q_{ki}\sigma^*_{kl}Q_{lj} \text{ and } \sigma^*_{ij} = Q_{ik}\sigma_{kl}Q_{jl} \tag{4.1}$$

where Q_{ij} describe a rigid body rotation.

Now taking the material derivate of (4.1)

$$\frac{D\sigma^*_{ij}}{Dt} = \frac{DQ_{ik}}{Dt}\sigma_{kl}Q_{jl} + Q_{ik}\frac{D\sigma_{kl}}{Dt}Q_{jl} + Q_{ik}\sigma_{kl}\frac{DQ_{jl}}{Dt} \tag{4.2}$$

It is evident that the tensor quantity $D\sigma_{kl}/Dt$ is not objective. To obtain a valid objective stress rate, (3.40) is useful. The spatial velocity gradient can be expressed as

$$L^*_{ij} = \frac{DQ_{ik}}{Dt}Q_{jk} + Q_{ik}L_{kl}Q_{jl} \tag{4.3}$$

and the expression of the rate-of-deformation as an objective tensor becomes

$$D^*_{ij} = Q_{ik}D_{kl}Q_{jl} \tag{4.4}$$

Now the spin tensor (3.40) with (4.3) and (4.4) can be expressed as

$$W^*_{ij} = Q_{ik}W_{kl}Q_{jl} + \frac{DQ_{ik}}{Dt}Q_{jk} \tag{4.5}$$

Use of (4.2) and (4.5) gives

$$\frac{D\sigma^*_{ij}}{Dt} = \left(W^*_{ik}Q_{kl} - Q_{ik}W_{kl}\right)\sigma_{lm}Q_{jm} + Q_{ik}\frac{D\sigma_{kl}}{Dt}Q_{lj} + Q_{ik}\sigma_{kl}\left(Q_{ml}W^*_{jm} - W_{ml}Q_{jm}\right) \tag{4.6}$$

this with (4.1) may be written as

$$\frac{D\sigma_{ij}^{*}}{Dt} - W_{ik}^{*}\sigma_{kj}^{*} - \sigma_{ik}^{*}W_{jk}^{*} = Q_{ik}\left(\frac{D\sigma_{kl}}{Dt} - W_{km}\sigma_{ml} - \sigma_{km}W_{lm}\right)Q_{jl} \tag{4.7}$$

It appears that one can define following objective quantity from (4.7)

$$\sigma_{ij}^{\nabla J} = \frac{D\sigma_{ij}}{Dt} - W_{ik}\sigma_{kj} - \sigma_{ik}W_{jk} \tag{4.8}$$

This expression is commonly known as the Jaumann rate of the Cauchy stress. Now the material derivate of Cauchy stress consists of two parts: the rate of change due to material response, which is reflected in the objective rate, and the change of stress due to rotation, which corresponds to the two last terms in (4.8).

To prove that frame indifference is not only a mathematical problem, a realistic example will follow.

Consider a bar that is initially loaded with a constant stress of σ_0. An observer that is riding with the body during a rotation (rigid body motion) of a bar in time will not observe any difference in stress, the initial value remains, Figure 4.1.
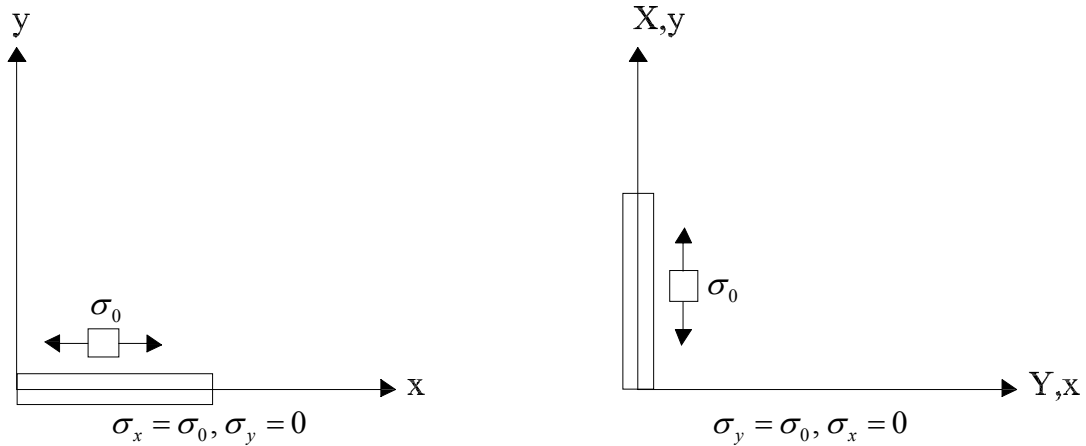

Figure 4.1: Rotation of a bar under initial stress.

Since no deformation has occurred during the rotation, the rate-of-deformation D_{ij}, equals zero, which is a correct assumption, but undecidedly leads to that $D\sigma_{ij}/Dt = 0$ which is incorrect see (4.2). The components of Cauchy stress in a fixed coordinate system will change during the rotation, so the material derivative of the stress must be nonzero. Obviously, something is missing in equation (4.2) since it does not support rigid-body-motions.

The material rotation can be accounted for an objective rate of the stress tensor or often called a *frame-invariant rate*. There exist several objective rates, some more commonly are Truesdell-rate and Green-Naghdi-rate among others, but throughout this work all derivations are based on the Jaumann-rate.

4.2 Elasticity at finite strain

4.2.1 Hypo-elasticity

Hypo-elastic laws are used primarily for representing the elastic response in elasto-plastic material laws, where the elastic deformations are small. The most common elasto-plastic constitutive models that are implemented into conventional FE-programs are based upon Hypo-elasticity. The theory presented in chapter 4.2.1 and 4.2.2 is taken from [6], if nothing else is indicated.

Hypo-elastic material laws relate the rate of stress to the rate of deformation. A general expression of Hypo-elasticity is given by

$$\sigma_{ij}^{\nabla} = g_{ij}\left(\sigma_{kl}, D_{kl}\right) \tag{4.9}$$

where σ_{ij}^{∇} represents any objective rate of the Cauchy stress tensor. The function g_{ij} must also be an objective function of the stress and rate-of-deformation.

Several of the Hypo-elastic constitutive relations can be expressed as linear relations between the objective measure of stress and the rate-of-deformation

$$\sigma_{ij}^{\nabla J} = C_{ijkl} D_{kl}^{e} \tag{4.10}$$

where $\sigma_{ij}^{\nabla J}$ is the Jaumann rate of Cauchy stress, D_{kl}^{e} is the elastic part of (3.41) and C_{ijkl} is the fourth-order elastic-moduli-tensor. This tensor can be expressed for an isotropic condition as

$$C_{ijkl} = \lambda \delta_{ij} \delta_{kl} + \mu\left(\delta_{ik} \delta_{jl} + \delta_{il} \delta_{jk}\right) \tag{4.11}$$

where λ and μ are the Lames constants.

With a hypo-elastic formulation an undesired effect arises during a large elastic strain application. The strain energy is not necessarily conserved, i.e. the work done in a closed elastic deformation path is not necessarily zero, Figure 4.2.
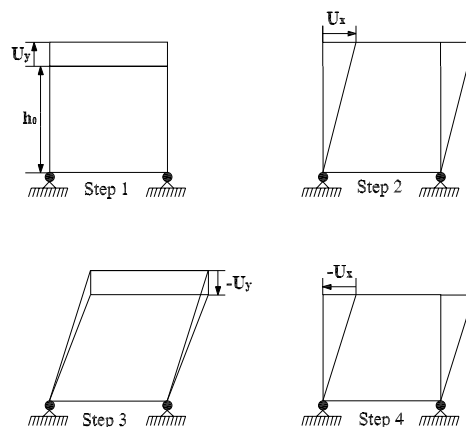

Figure 4.2: Closed deformation path in a four step illustration.

4.2.2 Hyper-elasticity

Hyper-elastic or often called Green elastic materials provide a natural frame-work for frame-invariant formulation [6], the frame indifference restrictions are trivially fullfilled if proper deformation measures are employed. Hyper-elasticity is a good model for non-linear elasticity, since the drawbacks of hypo-elasticity are avoided. Following expressions are taken from [18].

The second *Piola-Kirchoff* stress tensor, S_{ij}, and the rate of *Lagrangian* strain tensor, $\dot{E}_{ij}$, are conjugated quantities and therefore the strain-energy per unit reference volume can be expressed as

$$W(E_{ij}) = \int_0^{E_{ij}} S_{ij}(\widetilde{E}_{kl}) d\widetilde{E}_{ij} \qquad (4.12)$$

The notation $\widetilde{E}_{ij}$ indicates that it is an integration variable. From (4.12) an energy increment can be expressed as

$$dW = S_{ij} dE_{ij} \qquad (4.13)$$

The energy increment can also be expressed as

$$dW = \frac{\partial W}{\partial E_{ij}} dE_{ij} \qquad (4.14)$$

With (4.13) and (4.14) the following expression holds

$$S_{ij} = \frac{\partial W}{\partial E_{ij}} \quad where \quad W = W(E_{ij}) \qquad (4.15)$$

It appears that the strain energy W serves as a potential-function for the stresses. Choosing, for instance

$$W = \frac{1}{2} E_{ij} L_{ijkl} E_{kl} \qquad (4.16)$$

where L_{ijkl} is the positive definite constant *stiffness tensor*, results in the following simple hyper-elastic model

$$S_{ij} = L_{ijkl} E_{kl} \qquad (4.17)$$

4.3 Plasticity theory

Plasticity theory provides a mathematical relationship that characterizes the elasto-plastic response of materials. There are three ingredients in plasticity theory [3]: the yield criterion, hardening rule and the flow rule. The theory throughout chapter 4.3 is taken from [19], if nothing else is indicated.

4.3.1 Yield criterion

The yield criterion determines the stress level at which yielding is initiated. It is convenient to define a scalar function $F,$ as the yield criterion. If it is assumed that the material is isotropic, it does not have any preferred directions. Therefore, the *initial yield surface* can be expressed in terms of principal stresses [11]

$$F = F(\sigma_{ij}) = F(\sigma_1, \sigma_2, \sigma_3) = 0 \tag{4.18}$$

This can also be expressed in terms of the invariants of the stress tensor as [11]

$$F = F(J_1, J_2, J_3) = 0 \tag{4.19}$$

where $J_1,$ J_2 and J_3 are the invariants of the stress tensor and are defined by

$$J_1 = s_{ii}; \quad J_2 = \frac{1}{2} s_{ij} s_{ji}; \quad J_3 = \frac{1}{3} s_{ij} s_{jk} s_{ki} \tag{4.20}$$

where s_{ij} is the deviatoric stress tensor defined by

$$s_{ij} = \sigma_{ij} - \frac{1}{3} \sigma_{kk} \delta_{ij} \tag{4.21}$$

Since the yield surface in general varies with the increase of plastic strains, it is possible to express the *current yield surface* by

$$f(\sigma_{ij}, K^\alpha) = 0 \quad \alpha = 1,2,.. \tag{4.22}$$

where the so-called *hardening parameters* K^α are introduced. That characterizes the way in which the current yield surface changes its size, shape and position with plastic loading.

The number of hardening parameters is unknown at the moment but as indicated; it is permitted to have more than one.

The type of the hardening parameters may be scalars or higher-order tensors. Initially the hardening parameter is set to zero, this means that the current yield surface coincides with the initial yield surface. The choice of hardening parameters therefore implies a choice of hardening rule.

The hardening parameters K^α vary with the plastic loading. To model this, it is assumed that there exist some internal variables that are used to memorize the plastic loading history. In analogy with the notation above, let κ^β denote the internal variables

$$\kappa^\beta = internal\ variables\ (\beta = 1,2...) \tag{4.23}$$
$$\kappa^\beta = 0\quad initially$$

Because the internal variables memorize the plastic loading history, they are zero before any plasticity is initiated. Since the internal variables κ^β characterize the elastic-plastic material, the hardening parameter K^α depend on the internal variables κ^β

$$K^\alpha = K^\alpha(\kappa^\beta) \tag{4.24}$$

4.3.2 Hardening rule

The hardening rule describes the changing of the yield surface with increasing yielding. Three common hardening rules are: perfectly plastic, isotropic hardening and kinematic hardening.

Thermoplastic materials often experience hardening during plastic straining. If a material is assumed not to experience hardening during plastic straining, the yield surface is unaffected by the plastic deformations, then it is called *perfectly plastic* [11].

Yield criteria for this type of material can be expressed with (4.22) as

$$f(\sigma_{ij},0) = F(\sigma_{ij}) = 0 \tag{4.25}$$

During plastic straining the shape, size, and orientation of the yield surface remain unchanged as shown in Figure 4.3.
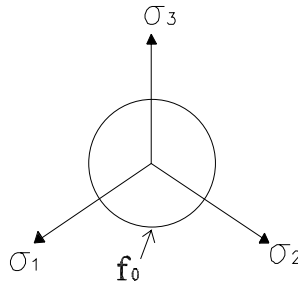

Figure 4.3: Perfectly plastic.

The initial yield surface f_0 is often defined as the locus of stress states when the first yielding occurs shown in Figure 4.3, inside the surface the stresses are elastic and the material behaves elastically.
If an initially isotropic material hardens isotropically, the yield condition can be expressed as

$$f(\sigma_{ij},K^\alpha) = F(\sigma_{ij}) - K^\alpha = 0 \tag{4.26}$$

In other words, as hardening occurs, the value of $K^{\alpha}(\kappa^{\beta})$ and the size of the yield surface changes with the development of plastic strains, shown in Figure 4.4. This event, will not affect the shape or orientation.
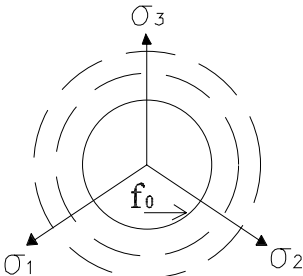

Figure 4.4: Isotropic hardening.

In mathematical terms, hardening is obtained by letting the function $K^{\alpha}(\kappa^{\beta})$ in (4.26) increase with increasing plastic deformation. If the function $K^{\alpha}(\kappa^{\beta})$ at some stage decreases with increasing plastic deformation then the yield surface shrinks in size corresponding to softening plasticity.

As illustrated in Figure 4.5, if the loading is reversed from point A where $\sigma = \sigma_y$, the isotropic hardening model will predict elastic unloading until point B is reached. The isotropic hardening model predicts the same yield stress in tension and in compression. For some materials, experimental results show that point B, where plastic effects again are encountered, occurs much earlier than predicted. This effect is called the Bauschinger effect.
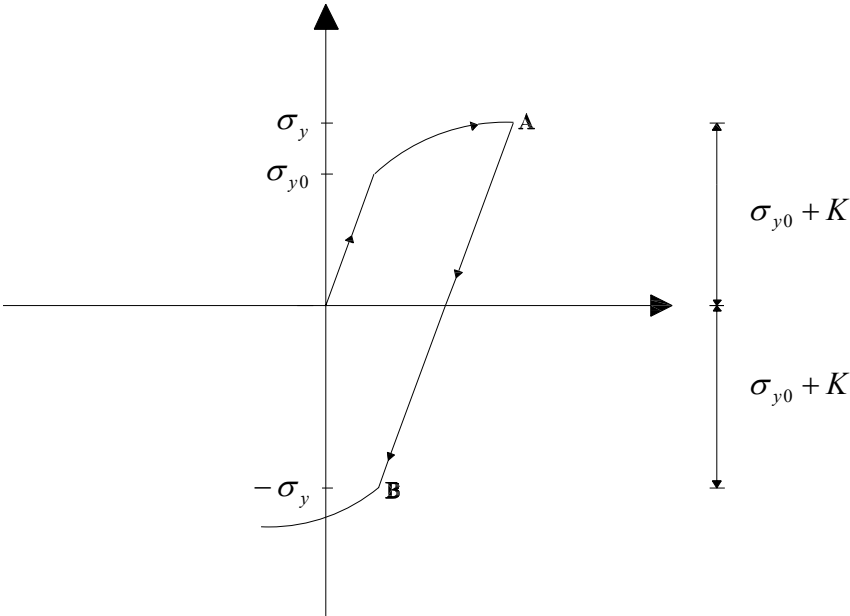

Figure 4.5: Isotropic hardening.

A way to approximate the Bauschinger effect is to assume that the difference between the two yield points is the value of $2\sigma_{y0}$, cf. Figure 4.6. This approximation of hardening is called *kinematic hardening.*
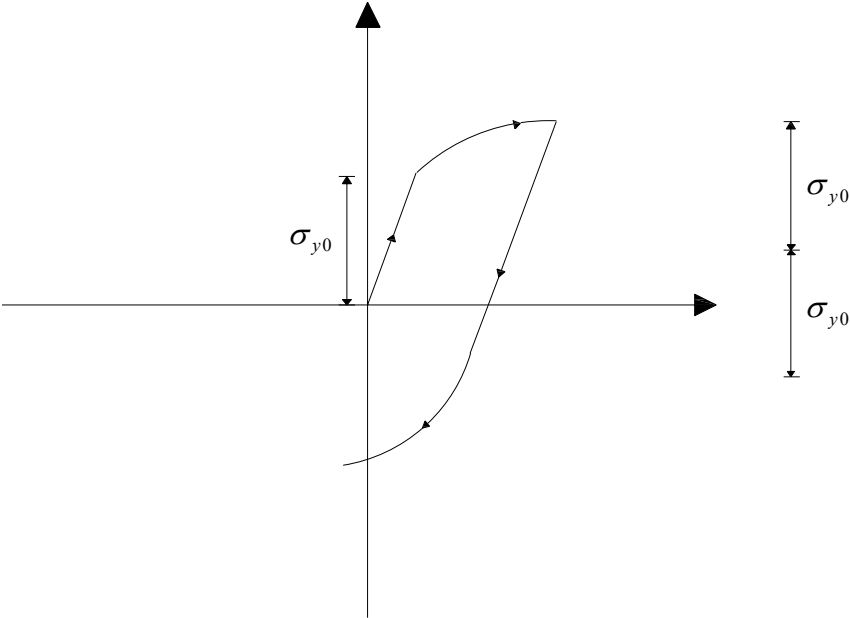

Figure 4.6: Kinematic hardening.

The idea of kinematic hardening is that the shape and size of the yield surface remain the same but the yield surface can translate in the direction of the plastic strain increment in the stress space, Figure 4.7.
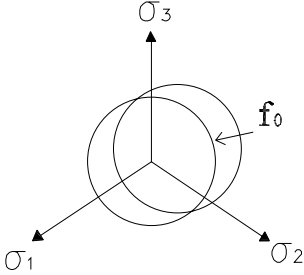
Figure 4.7: Kinematic hardening.

During plastic deformations the yield surface can be expressed as

$$f(\sigma_{ij}, K^\alpha) = F(\sigma_{ij} - \alpha_{ij}) = 0 \tag{4.27}$$

where the hardening parameter in terms of the tensor α_{ij} represents total translation of the yield surface. A more general hardening is obtained if the two models are combined into mixed hardening, i.e. both the size and the position of the yield surface are allowed to change.

4.3.3 Flow rule

When the state of stress reaches the yield surface f, the material undergoes plastic deformation; this is also called plastic flow [11], which is defined through a flow rule.

The flow rule determines the direction of plastic straining and can be given as [3]

$$D_{ij}^p = \dot{\lambda} \frac{\partial Q}{\partial \sigma_{ij}} \tag{4.28}$$

where D_{ij}^p is the plastic part of (3.41) and $\dot{\lambda}$ is the plastic multiplier, which determines the amount of plastic straining. Q is the plastic potential function which determines the direction of plastic flow direction.

If Q is the yield function, the flow rule is referred to as an *associative flow* rule of plasticity [11] and the plastic strains occur in a direction normal to the yield surface [3]. Many materials are best modelled when the yield surface f and the plastic potential function Q are different.

In the same way as in the flow rule, it is possible to establish a flow rule for the internal variables.

$$\dot{\kappa}^\alpha = \dot{\lambda} \frac{\partial Q}{\partial \mathrm{K}^\alpha} \tag{4.29}$$

4.4 Hypo-elastic-plastic constitutive model

The elasto-plastic constitutive models that ANSYS uses today are based upon hypo-elastic-plastic models. This model is an extension of hypo-elasticity, described in chapter 4.2.1. Following expressions are taken from [6].

The modelling of plasticity for large strains often implies an additive split of the rate of deformation, D_{ij} into an elastic part and a plastic part

$$D_{ij} = D_{ij}^e + D_{ij}^p \tag{4.30}$$

With (4.10) and (4.30) the *Jaumann-rate* can be expressed as

$$\sigma_{ij}^{\nabla J} = C_{ijkl,el} \left(D_{kl} - D_{kl}^p \right) \tag{4.31}$$

If the elastic moduli, $C_{ijkl,el}$, is assumed to be constant, it must be isotropic in order to satisfy the principle of material frame indifference.

Now introducing one important feature for Jaumann-rate, that $(f_\sigma)_{ij}$ and σ_{ij} is commute. This leads to the following relationships

$$\left(f_\sigma \right)_{ij} \sigma_{kl} = \sigma_{ij} \left(f_\sigma \right)_{kl} \text{ and } \left(f_\sigma \right)_{ij} \dot{\sigma}_{kl} = \left(f_\sigma \right)_{ij} \sigma_{kl}^{\nabla J} \tag{4.32}$$

Using the consistency relation $\dot{f} = 0$ from (4.22) with the relation (4.31), the plastic flow relation (4.28), the evolution equation (4.29) and the relation (4.32) gives the consistency condition

$$\dot{\lambda} = \frac{(Q_\sigma)_{ij} C_{ijkl,el} D_{kl}}{-(Q_K)_\alpha h_\alpha + (Q_\sigma)_{rs} C_{rstu,el} r_{tu}} \tag{4.33}$$

where $r_{ij} = \partial f / \partial \sigma_{ij}$ is the plastic flow direction and $h_\alpha = \partial f / \partial K^\alpha$ is the flow direction for internal variables. For an associative flow rule $(Q_\sigma)_{ij} = (f_\sigma)_{ij}$.

4.5 Rate-dependent plasticity

For many materials like thermoplastic materials, the strain rate influences the material behaviour, which necessitates a separation of this behaviour into rate-dependent and rate-independent. Materials where the stress-strain response is independent of the rate of deformation, is said to be rate-independent, Figure 4.8a; otherwise rate-dependent, Figure 4.8b.

In a large class of rate-independent and rate-dependent elastic-plastic constitutive equations the elasticity is modelled in hypo-elastic form, with the stress rate being taken as the Jaumann derivative, so as to make the constitutive model properly frame-indifferent or objective [2].
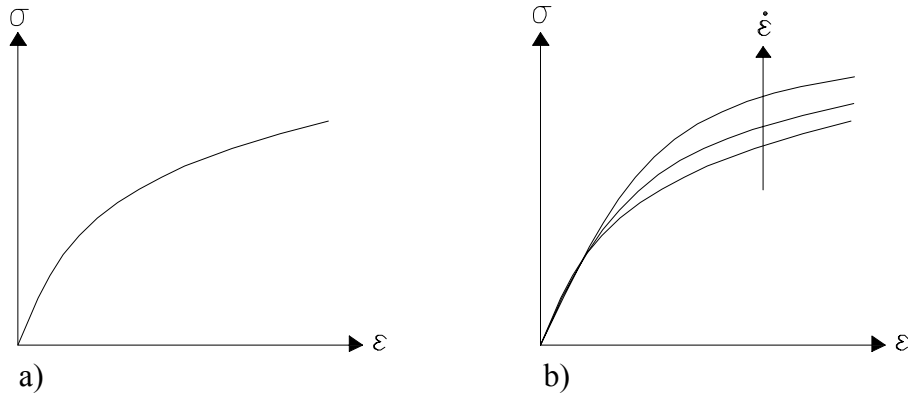

Figure 4.8: Engineering stress-strain curve a) rate-independent material b) rate-dependent material.

The addition of viscous effects to the derived hypo-elastic-plastic model in chapter 4.4, is just an adjustment of the plastic rate parameter $\dot{\lambda}$. This will now be expressed as [6]

$$\dot{\lambda} = \frac{\Phi(\sigma_{ij}, K)}{\eta} \tag{4.34}$$

where $\Phi(\sigma_{ij}, K)$ is an overstress function and η is the viscosity. It shall be pointed out that the over stress function has the dimension of stress and can be considered as the driving force for the plastic strain [6]. To get a grip of how a rate-dependent model is composed, a one dimensional rheological model will be considered, Figure 4.9.
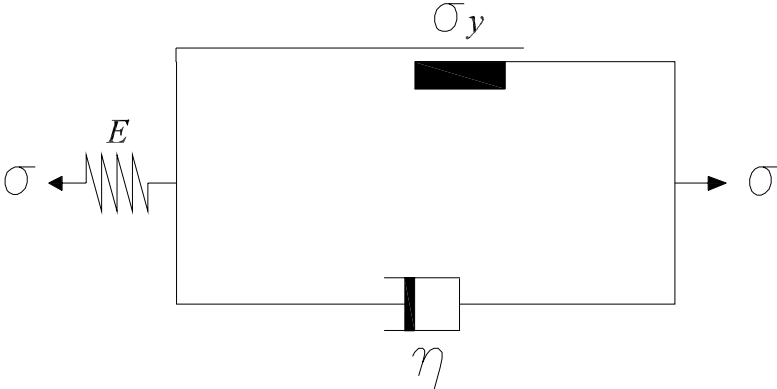

Figure 4.9: One dimensional rheological model.

The constant frictional stress is represented by σ_y, η is the viscous constant and E is the elastic constant [14]. Thermoplastic materials in general have a material behaviour that combines all above described, Figure 4.9.

4.5.1 Viscosity models

In this thesis, there was a limit of the available numbers of material models implemented in ANSYS, which support the plastic and viscous behaviour of PC/ABS. There are only three models in ANSYS that support visco-plasticity, Anand's model, Peirce model and Perzyna model. Of those models mentioned above, there are only two material options available that are suitable for large strain rates, namely the Perzyna and the Peirce model. Both of these models must be combined with isotropic hardening. Another requirement is that the material model has to be able to describe the typical softening behaviour, cf. Figure 4.10
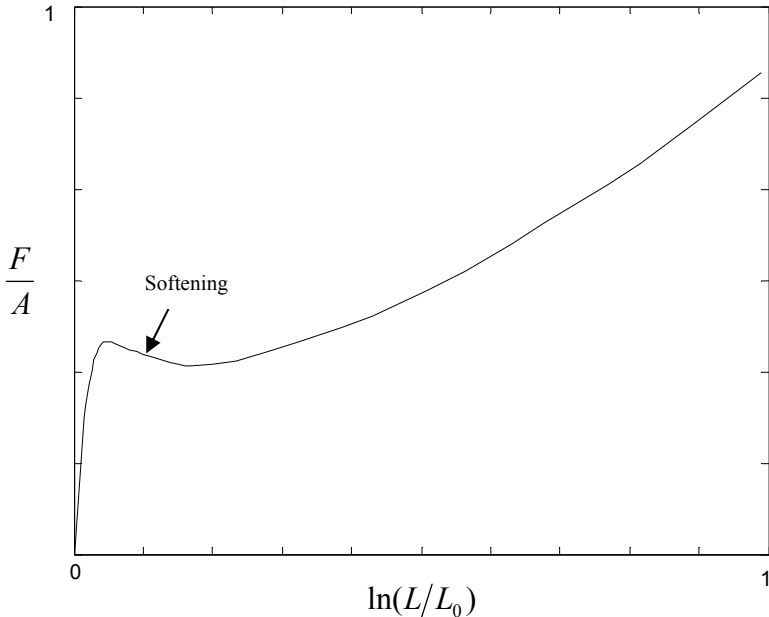

Figure 4.10: Softening behaviour.

One drawback for these models is that the strain rate effects are only active after plastic yielding has occurred [3] and it can not describe viscous effects during unloading.

In a more detailed fashion, the models can be described as follows [3].

The visco-plastic flow rule is given as

$$D_{ij}^p = \gamma \left(\frac{\sigma_y}{\sigma_0} - 1 \right)^n \frac{\partial f}{\partial \sigma_{ij}}$$

(4.35)

for Perzyna model and

$$D_{ij}^p = \gamma \left(\left(\frac{\sigma_y}{\sigma_0} \right)^n - 1 \right) \frac{\partial f}{\partial \sigma_{ij}}$$

(4.36)

for Peirce model, where σ_y is the yield stress, σ_0 is the static initial yield stress, n is a hardening parameter and γ is the viscosity parameter.

The equivalent-plastic-strain rate is based on the visco-plastic flow rule as follows

$$\dot{\varepsilon}_{eqv}^p = \sqrt{\frac{2}{3} D_{ij}^p D_{ij}^p} = \gamma \left(\frac{\sigma_y}{\sigma_0} - 1 \right)^n$$

(4.37)

for Perzyna model and as

$$\dot{\varepsilon}_{eqv}^p = \sqrt{\frac{2}{3} D_{ij}^p D_{ij}^p} = \gamma \left(\left(\frac{\sigma_y}{\sigma_0} \right)^n - 1 \right)$$

(4.38)

for Peirce model.

5 Material testing

The choice of material model is important and may not always be obvious. To understand the behaviour of the thermoplastic, it is necessary to perform material testing. A good way to evaluate material behaviour is to do tensile tests at different rates. This will, among other things, show viscous effects in the material. Some of the material properties are provided by the material supplier, but they need to be complemented with further material tests.

5.1 The stress-strain curve

A uniaxial (one dimensional) stress-strain curve can be obtained from a tensile test. Often the applied load versus elongation is illustrated without any attention taken to the geometrical behaviour during loading. In order to extract meaningful information about the material behaviour from the tensile tests, all effects of the specimen geometry needs to be eliminated.

For materials where the strains are just a few percent, the cross section area decrease is not significant; in those cases the cross section area will be approximated to be constant. This is not the case for thermoplastic materials, where many load applications results in large strains and hence the cross section area can not be approximated as constant, cf. Figure 5.1. The following definitions are taken from [6].
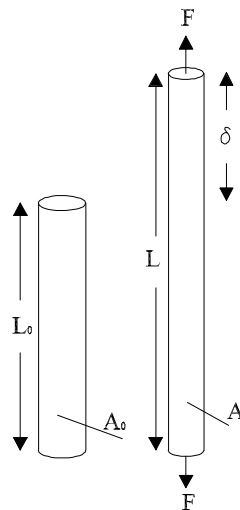

Figure 5.1: Geometrical behaviour during loading

Where the cross section area is approximated as constant, the mechanical response is often expressed in *Engineering stress* and *Engineering strain*. Define the stretch as

$$\lambda = \frac{L}{L_0} \tag{5.1}$$

where $L = L_0 + \delta$ is the length of the gage section associated with elongation δ. The engineering strain is then defined as

$$\varepsilon_0 = \frac{\delta}{L_0} = \lambda - 1 \tag{5.2}$$

The nominal or engineering stress is given by

$$\sigma_0 = \frac{F}{A_0} \tag{5.3}$$

where A_0 is the original cross-sectional area.

If the cross section area change is significant, *true stress* must be considered instead of the engineering stress.

$$\sigma = \frac{F}{A} \tag{5.4}$$

where *A* is the current cross section area, i.e. not approximated to be constant any longer.

The strain, ε, can be measured by integrating the change of unit current length. This measure of strain is called *true strain* or *logarithmic strain*.

$$\varepsilon = \int_{L_0}^{L} \frac{1}{L} dL = \ln\left(\frac{L}{L_0}\right) = \ln(\lambda) \tag{5.5}$$

The time derivate of the logarithmic strain (5.5) will in one-dimensional case be equal to the rate of deformation.

$$\dot{\varepsilon} = \frac{\dot{\lambda}}{\lambda} = D_{11} \tag{5.6}$$

The nominal strain rate is defined as

$$\dot{\varepsilon}_0 = \frac{\dot{\delta}}{L_0} \tag{5.7}$$

Since

$$\dot{\delta} = \dot{L} \text{ and } \frac{\dot{\delta}}{L_0} = \frac{\dot{L}}{L_0} = \dot{\lambda} \tag{5.8}$$

it follows that the nominal strain rate is equivalent to the rate of stretching, i.e. $\dot{\varepsilon} = \dot{\lambda}$, in a one dimensional case. This relation is not true for general multiaxial states of deformation, unless the principal axes of the deformation are fixed.

5.2 The plastic behaviour

Many polymers that undergo loading above the yield stress stretch uniformly for a few percent and then, instead of breaking, they fail by forming a neck. The neck may get steadily thinner until break, or it may stabilize at some point and then the shoulders travel along the specimen. In this case, the phenomenon is called cold-drawing [17] [22].

Necking is a geometrical behaviour, which typically starts before the softening on the engineering stress-strain curve. Furthermore strain will change the softening process into a hardening process until failure [1] [12] [13].

Another interesting feature of thermoplastic materials is that they show a different behaviour when they are exposed to compression compared to tension. When looking at Polycarbonate, PC, which is a component of PC/ABS, this effect is obvious, cf. Figure 5.2. The response in tension is significantly stiffer than in compression [4].
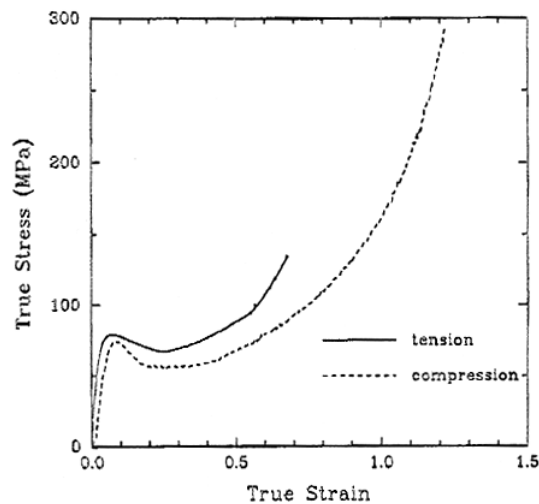
Figure 5.2: PC [4].

5.3 Data from the material supplier

Figures 5.3 and 5.4 show data from the supplier of PC/ABS at different temperatures and load rates. Figure 5.3 show tensile tests at 23° C at different load rates. It has typical strain rate-dependence, since the load rate influence the load level for necking entry.
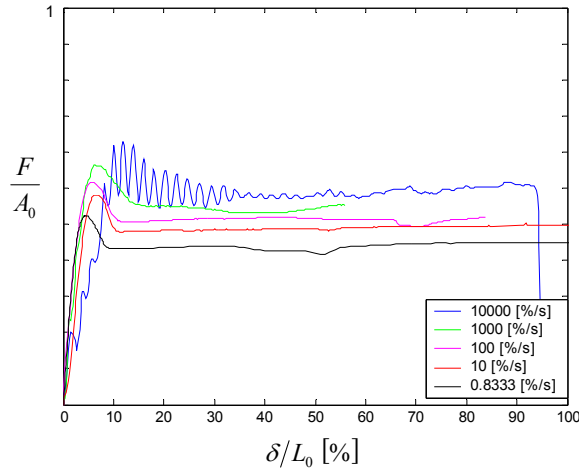

Figure 5.3: Tensile tests of PC/ABS at different load rates and a temperature of $23^\circ C$.
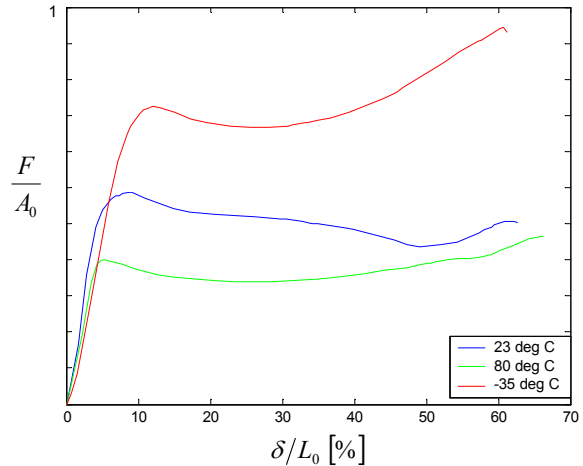

Figure 5.4: Compression tests of PC/ABS at different temperatures.

In Figure 5.4, a compression test has been made at different temperatures. Intuitive the material manage more load when cooled compared to a heated level.

Under uniaxial compressive loading conditions, the underlying polymeric network chain structure is undergoing a planar orientation process which gives rise to the corresponding observed strain hardening behaviour. The necked region of the tensile specimen is being cold drawn resulting in a uniaxial state of orientation. Therefore, the observed engineering strain hardening in uniaxial tension distinctly differs from that obtained in uniaxial compression, giving different stress-strain curves [8] [5].

5.4 The tensile test

In order to accurately model the material behaviour, a reliable set of experimental data over an adequate range of strain rates is required. The true stress-strain testing of polymers is a formidable task due to the difficulty of conducting such tests to very large strains while maintaining a homogeneous state of deformation [4].

5.4.1 Test preparation

All tensile tests were made at LTH with a tensile testing machine like the one in Figure 5.5, at normal temperature and pressure conditions.

Figure 5.5: MTS tensile testing machine.

The test specimen is injection-moulded and made of PC/ABS. The essential dimensions can be seen in Figure 5.6. 115 mm indicates the distance between the grips. Dimensions of the specimen follow the norm ISO 527-2/1A.
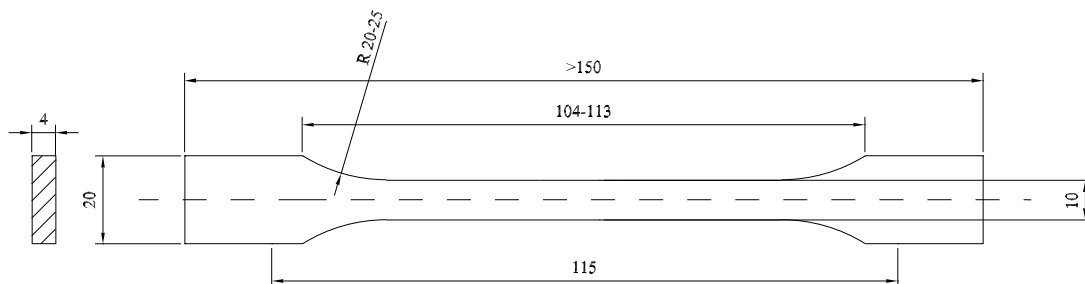

Figure 5.6: Test specimen ISO 527-2/1A.

5.4.2 Testing procedure

Tensile tests with constant displacement rate were performed on all test specimens for comparison with the simulated tensile test results from finite element analysis. A displacement controlled application was chosen because of the critical necking phase that would make the specimen collapse, if a load controlled application was chosen instead.

The test equipment measures applied displacement versus obtained load. This data can not directly be transformed to true stress and true strain, since the cross section area decreases with the strain. Due to the lack of test equipment that could measure this area decrease, we had to find this in another way, which will be described in chapter 6.

There is helpful equipment that can measure the cross section area, for example a CCD-camera. Even with this equipment this data is difficult to measure with accuracy, since the area decrease arises somewhere along the specimen during stretching and therefore one does not know where the area decrease takes place exactly. Unfortunately the material supplier could not support us with this data of true stress and true strain.

5.4.3 Results of tension tests

Results of the tension tests made at different strain rates are shown in Figure 5.7. Near the maximum force, the specimen creates a neck and a very rapid decrease in cross section area appears. Once the neck stabilizes locally, drawing continues as material is pulled from the wider regions. During this time the load cell records very little increase in force.
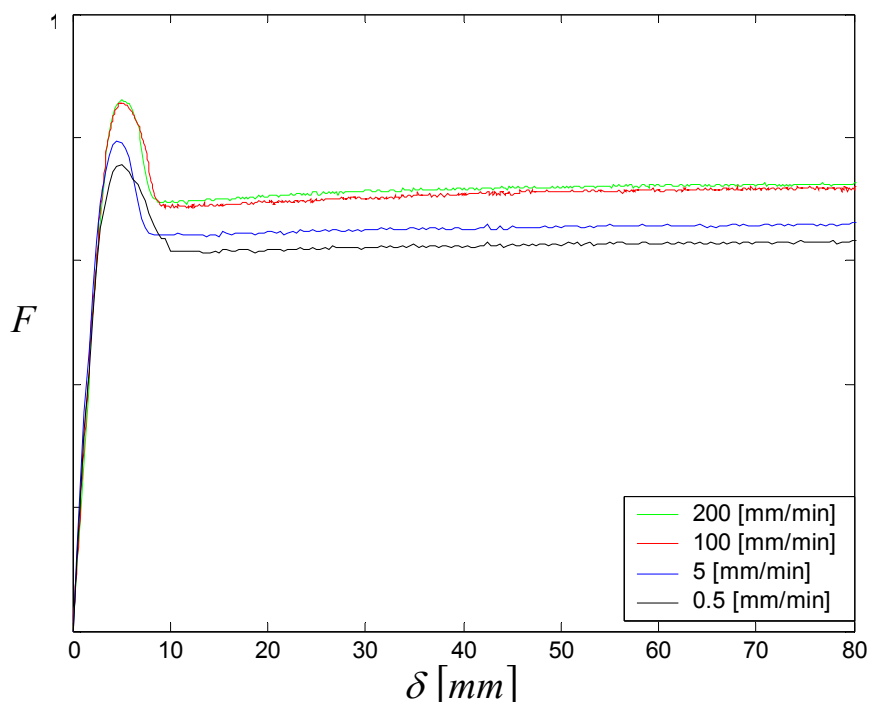

Figure 5.7: Tensile test at different rates for PC/ABS.

From the material supplier data, Figure 5.3, and from the tensile tests in Figure 5.7, it is obvious that the material behaves differently when exposed to varying strain rate. This indicates that the material is rate-dependent, which must be considered when choosing the material model. To evaluate the yield stress of PC/ABS one needs to do further material tests, where the rate-dependent contribution is eliminated. Due to this a static tensile test was done, cf. Figure 5.8.

Unloading this static curve at midway will identify if there exists any remaining deformation, at this load level.
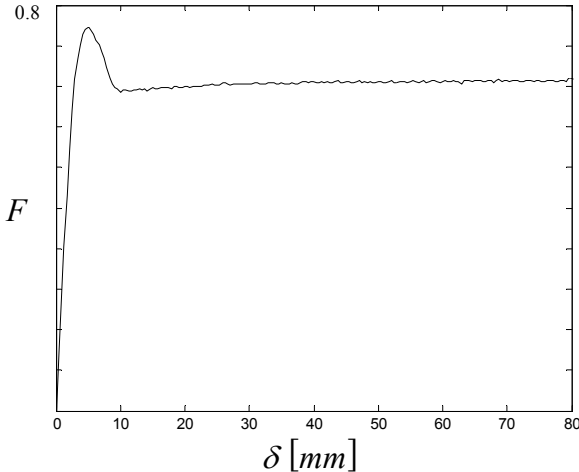

Figure 5.8: PC/ABS
loading at a rate of 0.5 mm/min
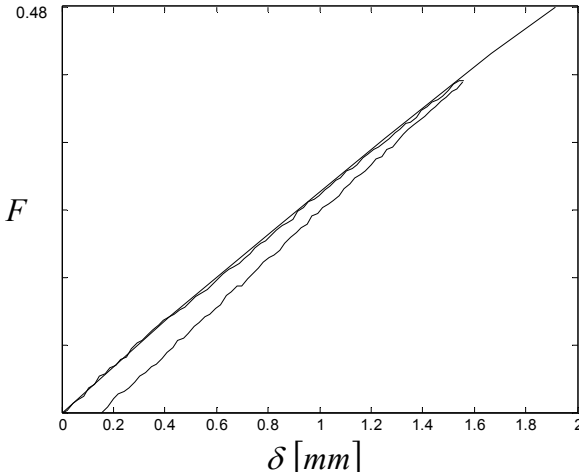
Figure 5.9: PC/ABS
Unloading at a rate of 0.5 mm/min

Obviously there exists a remaining deformation at this load level, Figure 5.9.

In metals an often used plastic limit is the so called *RP0.2 limit*, which occurs when 0.2% remaining plastic deformation exists after unloading. For materials like thermoplastics this entry is not so sharp and may be effects of the rate-dependence. This is the reason why an exact yield stress is hard to define for PC/ABS.

6 Calibration of the constitutive model

Material models are mathematical descriptions of material behaviour. For the adoption of the material model, one needs to determine several material parameters therefore experimental data is needed.

According to Figure 5.3 and 5.7, PC/ABS is showing rate-dependent effects. Due to lack of information, one does not know if the viscous effects exist in the elastic region.

The isotropic hardening is in ANSYS described by an input of a true stress-strain curve like the one in Figure 6.1. Before the calibration will be described, the procedure of numerical simulations must be explained.
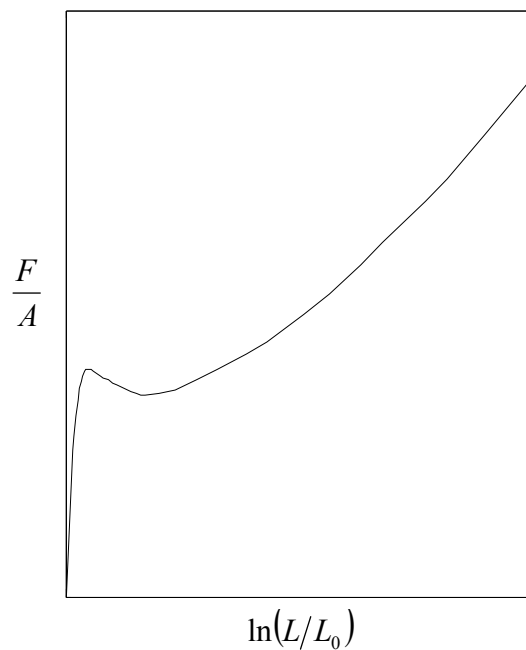

Figure 6.1: True stress versus true strain.

6.1 Numerical simulation of the uniaxial tensile testing of PC/ABS

6.1.1 Element type

All simulations in ANSYS made in this thesis are based upon the 3D-solid element, *Solid185*. This element has eight nodes, node I through P Figure 6.2, and each node has three degrees of freedom, UX, UY, UZ.

This element supports orthotropic behaviour [3]

Young's modulus, E_x, E_y, E_z.

Poisson's ratio, $\upsilon_x, \upsilon_y, \upsilon_z$ or the shear angle, $\gamma_x, \gamma_y, \gamma_z$.

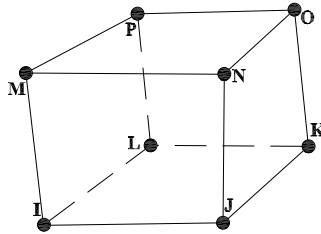Temperature dependence, $\alpha_x, \alpha_y, \alpha_z$.

Figure 6.2: Solid185

Other features that this element supports are plasticity, hyper-elasticity, creep, visco-plasticity, damping analysis and large strains [3].

6.1.2 Mesh

The simulated model of the tensile specimen represents the real one, with measurements according to Figure 5.6. Since there exist two planes of symmetry, only a quarter of the test specimen will be used, cf. Figure 6.3.
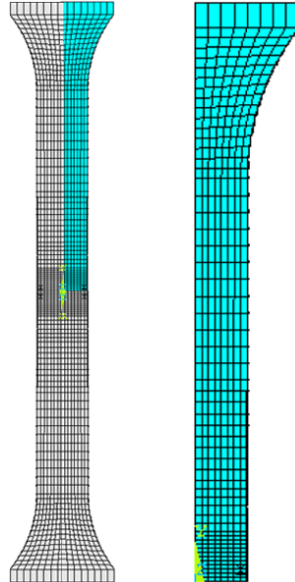

Figure 6.3: Finite element model of a
quarter of the tensile test specimen.

The use of symmetry planes reduces the simulation time noticeably. For many simulation applications, a 2-D model would be sufficient for Sony Ericsson. Unfortunately the simplification *plane-stress*, which could be an interesting alternative for simulations of cellular telephone shells, does not work for this model.

The mesh, which consists of 2640 elements, was divided in five regions, regarding element size. This was done to more easily change element size in sensible regions, if convergence problems occur. Since there exist large strains and thereby the elements are exposed to large stretching, one needs a tight mesh to avoid highly disordered elements. This will increase the calculation time, but otherwise maintain a reasonable accuracy of the simulation results.

6.1.3 Necking simulation

The simulated part has a necking behaviour in the same manner as a real test specimen. Since the narrowest width of the test specimen follows through over the whole test specimen, Figure 6.3a, a small imperfection was made to control the initial point of the necking. This imperfection of the test specimen was introduced in form of a width decrease of 1 % at the centre of the specimen (the bottom of the mesh), Figure 6.3b.

6.1.4 Boundary conditions

The nodes along the x- and y-axis of symmetry are constrained to have no displacement in U_y and U_x, respectively. The nodes located at the top of the specimen are constrained in U_z and prescribed to move in the vertical direction U_y, at a constant displacement rate corresponding to that applied in one of the actual experiments, cf. Figure 6.4.
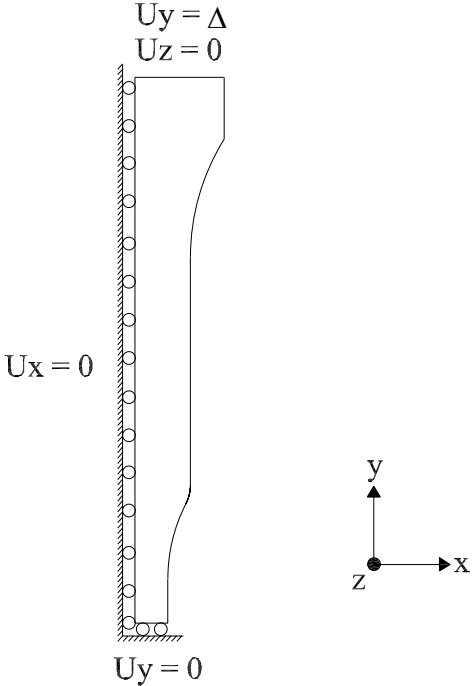

Figure 6.4: Test specimen, boundary conditions.

6.2 Modifying the input data

Usually all calculations are based upon engineering data in terms of engineering stress and engineering strain. In large strain analysis, generally stress-strain input is in terms of true stress and true strain. In small strain applications, the area reduction effect is insignificant and it will therefore not affect the accuracy of the simulation results.

From Figure 6.5, the curve with the slowest rate is considered as static in this thesis. This curve was also the base for the true stress-strain curve.
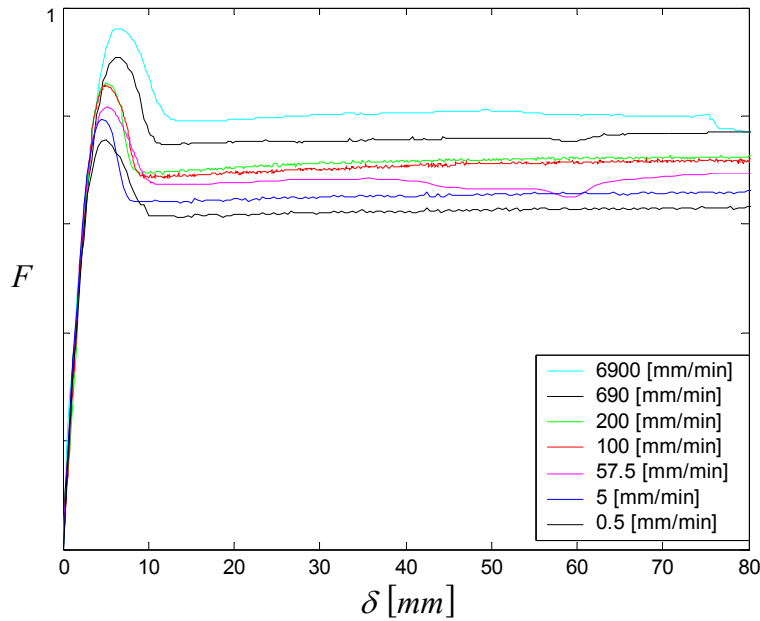

Figure 6.5: Tensile tests made at different rates for PC/ABS.

For small-strain regions of response, true strain and engineering strain are essentially identical. There is no efficient way to convert engineering stress to true stress, therefore an initial guess; an assumption from [3] was used

$$\sigma_{true} = \sigma_{eng}\left(1 + \varepsilon_{eng}\right) \tag{6.1}$$

This stress adaptation is valid only for incompressible plasticity. This is not the fact for the investigated thermoplastic where Poisson's ratio is not constant throughout the yield point due to cavitations [9]. Expression (6.1) should not be used after softening has been initiated due to the area decreasing. The adaptation to true stress and true strain after necking was therefore only a qualitative guess based upon earlier work see Figure 5.2.

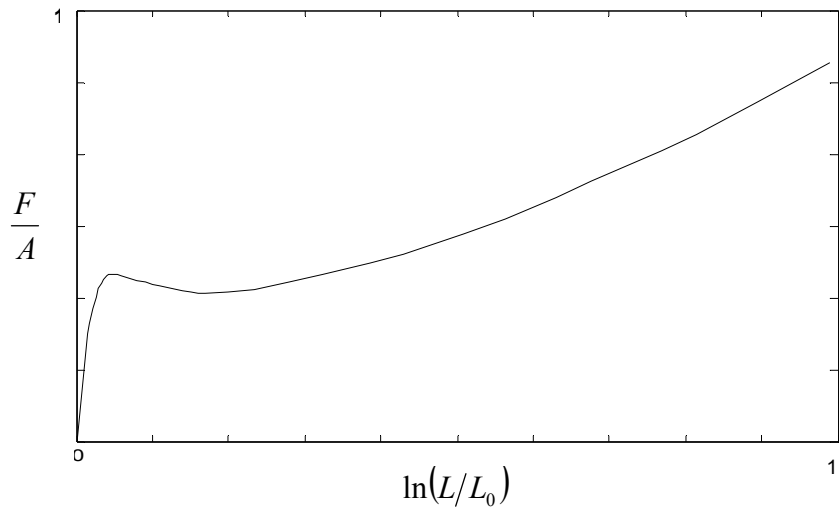The developed input data that is used throughout this thesis is illustrated in Figure 6.6.

Figure 6.6: Input data to ANSYS expressed in true stress and true strain.

6.3 Determination of viscosity parameters

Calibration of the rate-dependent behaviour, i.e. determination of the viscosity parameters, is an important aspect when simulating the behaviour of snaps or conducting simulations of drop tests, where the strain rates are high. Simulation programs, like ANSYS, require viscosity parameters to manage calculations at different strain rates.

6.3.1 The parameters m and γ

The next step is to calibrate the parameters m and γ in a satisfying manner. Rearranging (4.37) gives the Perzyna equation

$$\sigma_y = \left[1 + \left(\frac{\dot{\varepsilon}_{eqv}^{in}}{\gamma} \right)^m \right] \sigma_0 \tag{6.2}$$

Corresponding equation for Peirce (4.38) is

$$\sigma_y = \left[1 + \frac{\dot{\varepsilon}_{eqv}^{in}}{\gamma} \right]^m \sigma_0 \tag{6.3}$$

where:

σ_y = material yield stress

$\dot{\varepsilon}_{eqv}^{in}$ = equivalent plastic strain rate

$m = \dfrac{1}{n}$ = strain rate hardening parameter

γ = material viscosity parameter

σ_0 = static yield stress of material

As γ approach ∞, or m approach zero or $\dot{\varepsilon}_{eqv}^{in}$ approach zero, the solution converges to the static solution for Peirce. As γ approach ∞, or $\dot{\varepsilon}_{eqv}^{in}$ approach zero, the solution for Perzyna converges to the static solution. However, for this material option when m is very small (< 0.1), i.e. when a rate-independent model is approached, the solution shows difficulties in convergence [20].

To be able to find the parameters m (a value between 0 and 1) and γ (a value between 0 and ∞), it is first necessary to determine the material yield stress, static yield stress and equivalent plastic strain rate for as many tensile tests as possible.

Finding the yield stress for different strain rates is not an easy task with the given data. The only way is to make a qualified guess. By looking at tensile tests, see Figure 6.5, the yield stress is determined after the initial estimated linear part.

Figure 6.7 shows a comparison between Perzyna model (6.2) (dashed line) and determined yield stress as a function of strain rate (solid line).
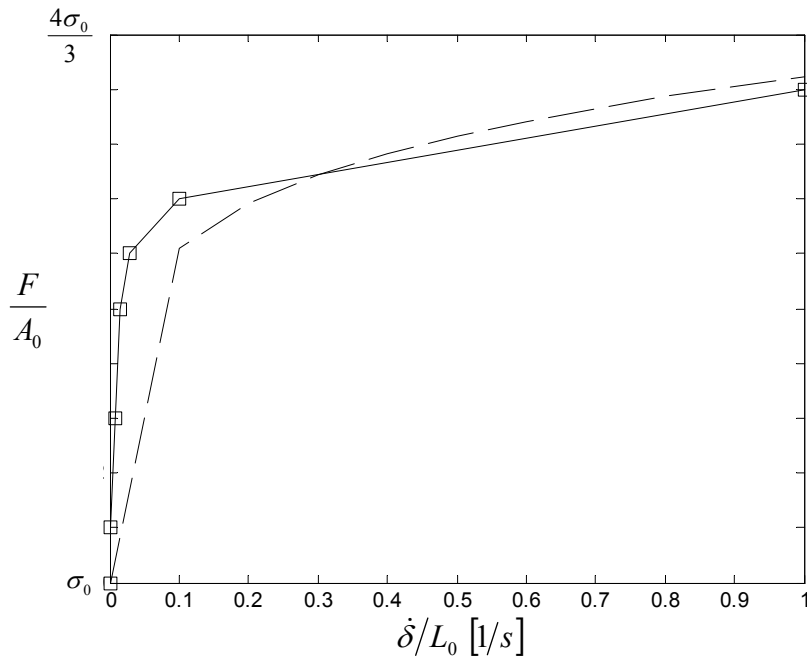
Figure 6.7: Yield stress as a function of strain rate (solid line) compared with Perzyna model (dashed line).

The determined yield stresses are only an estimate which will affect the values of m and γ noticeably.

Figure 6.8 shows a comparison between determined yield stress as a function of strain rate (solid line) and the Peirce equation (6.3) (dashed line).
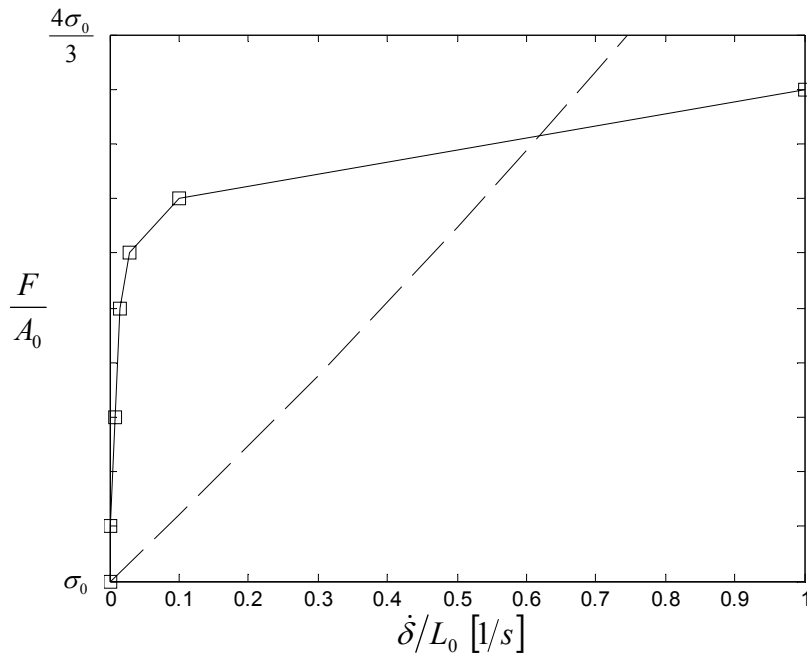

Figure 6.8: Yield stress as a function of strain rate (solid line) compared with Peirce model (dashed line).

It is not hard to see that no combination of m and γ will fit the Peirce model, so this model will be eliminated from further analysis.

Initially in the analysis, the Perzyna model with the chosen parameters of m and γ, was used, Figure 6.7. As mentioned above, these parameters only work as an initial estimation due to the difficulty in finding the yield stress. Tensile tests at different strain rates were simulated in ANSYS with the chosen parameters and compared with the real tests, Figure 6.5. If the results were not satisfying, new parameters were estimated and simulated for all strain rates in Figure 6.5 until an adequate result was achieved.

6.4 Results

The tensile tests were made at seven different strain rates, Figure 6.5, and compared with simulations made under the same conditions, Figure 6.9, 6.11, 6.12, 6.13, 6.15, 6.16 and 6.17

A typical plastic behaviour is the softening that occurs. This effect appears due to molecular rearrangement in the material. Describing this effect mathematically in a material model is difficult but has been achieved in this thesis, cf. Figure 6.10, 6.14 and 6.18. Simulations were done up to 80% global strains of the test specimen, with satisfying results. Of course, one must be aware of the limit when failure occurs.

The material model that has been investigated is a visco-plastic model. This material model describes the softening behaviour well, at an arbitrary rate. Figure 6.9, 6.11, 6.12, 6.13, 6.15, 6.16 and 6.17 show real tensile tests made in a tensile test machine, at different strain rates, compared with simulations of tensile tests made in ANSYS with the visco-plastic model.

Since we were testing the real specimen to failure, the same was done in the simulation. Unfortunately one does not know when break occurs in the simulation program, since the mesh keeps on stretching without notice. This is one of the reasons why one needs to do real tests to verify the validity of the simulation results.

The tensile specimen at Figure 6.10, 6.14 and 6.18 are scaled to fit in the same figure. This explains the differences in width of the tensile specimen.

Figure 6.9: A real test (solid line) of PC/ABS at a rate of 0.5
mm/min compared with simulation (dashed line).

The slowest tensile test was done at a displacement-rate of 0.5 mm/min, which was also the
selected curve that was stated to be static, Figure 6.9. It is obvious that the material model
with the chosen parameters of m and γ can not describe the softening acceptably for static
conditions, Figure 6.9. This drawback occurs because the Perzyna model approaches isotropic
hardening plasticity at slow strain rates. Isotropic hardening plasticity is not able to describe
this softening in a satisfying manner.

$\sigma_{Max} =$	70.5 MPa	76.7 MPa	80.3 MPa	82.2 MPa	84.9 MPa
$\sigma_{Min} =$	4.9 MPa	5.0 MPa	5.0 MPa	5.0 MPa	5.1 MPa
$U_{Max} =$	10.0 mm	20.0 mm	40.0 mm	60.0 mm	80.0 mm

Figure 6.10: Von Mises stress of PC/ABS at a rate of 0.5 mm/min. U_{Max} refers to global displacement.

The static result which was not totally satisfying, Figure 6.9, will not be a limitation for the material model, since in practical applications, static conditions are rare.

The typical area decreasing phenomenon for thermoplastic materials, the so called *cold-drawing* is illustrated in Figure 6.10.
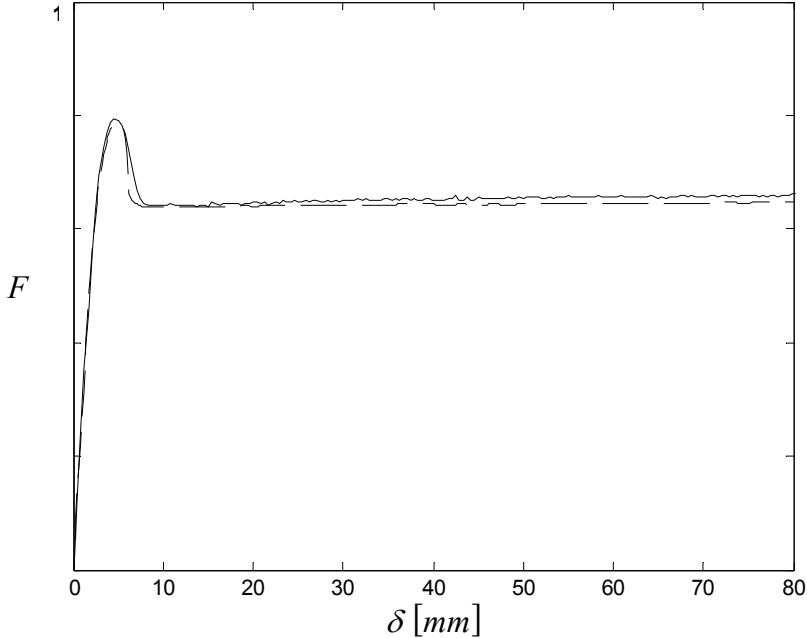

Figure 6.11: A real test (solid line) of PC/ABS at a rate of 5 mm/min compared with simulation (dashed line).

Already at a rate of 5 mm/min, the *Perzyna* model, describes the softening well, Figure 6.11.
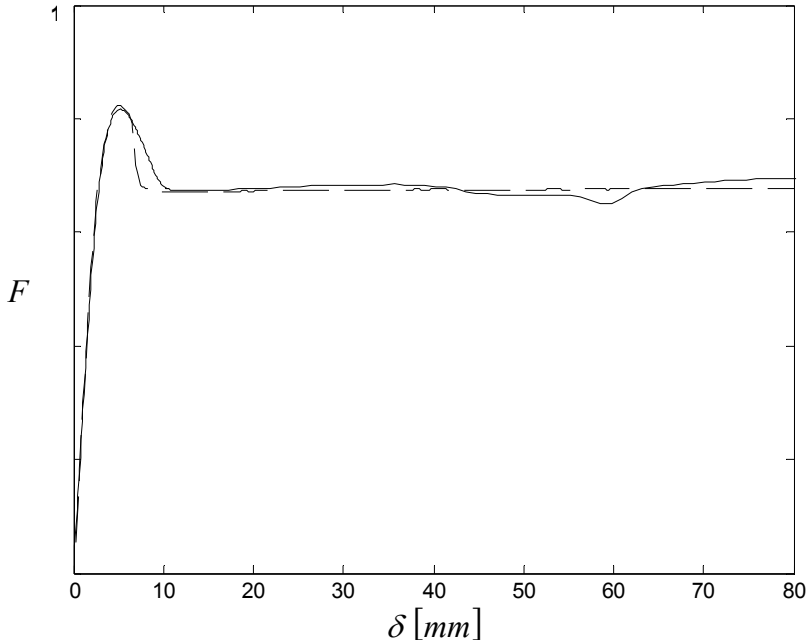

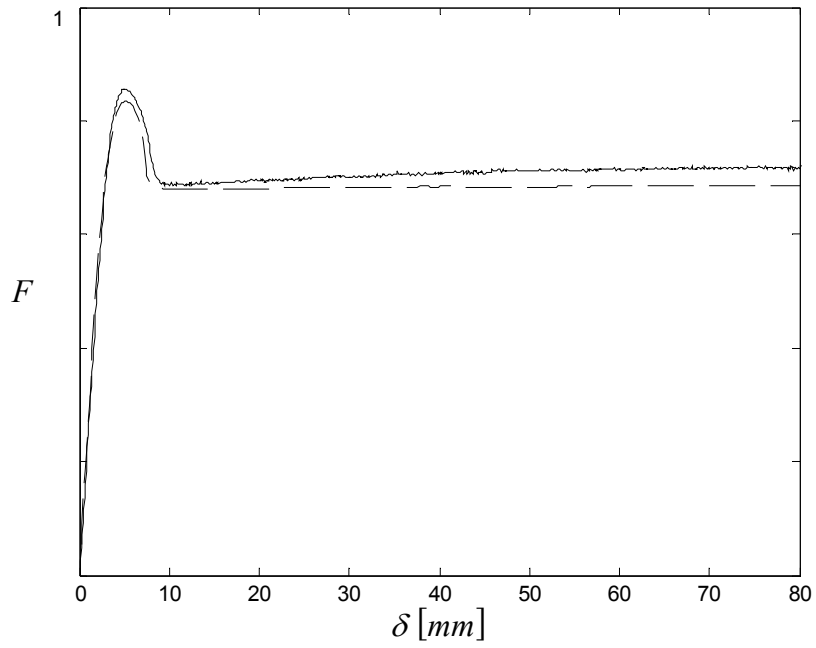**Figure 6.12:** A real test (solid line) of PC/ABS at a rate of 57.5 mm/min compared with simulation (dashed line).

43

Figure 6.13: A real test (solid line) of PC/ABS at a rate of 100 mm/min compared with simulation (dashed line).

$\sigma_{Max} =$	68.2 MPa	83.7 MPa	92.6 MPa	97.9 MPa	102.0 MPa
$\sigma_{Min} =$	5.6 MPa	5.6 MPa	5.6 MPa	5.6 MPa	5.6 MPa
$U_{Max} =$	10.0 mm	20.0 mm	40.0 mm	60.0 mm	80.0 mm

Figure 6.14: Von Mises stress of PC/ABS at a rate of 100 mm/min. U_{Max} refers to global displacement.

44

Figure 6.15: A real test (solid line) of PC/ABS at a rate of 200 mm/min compared with simulation (dashed line).

Figure 6.16: A real test (solid line) of PC/ABS at a rate of 690 mm/min compared with simulation (dashed line).
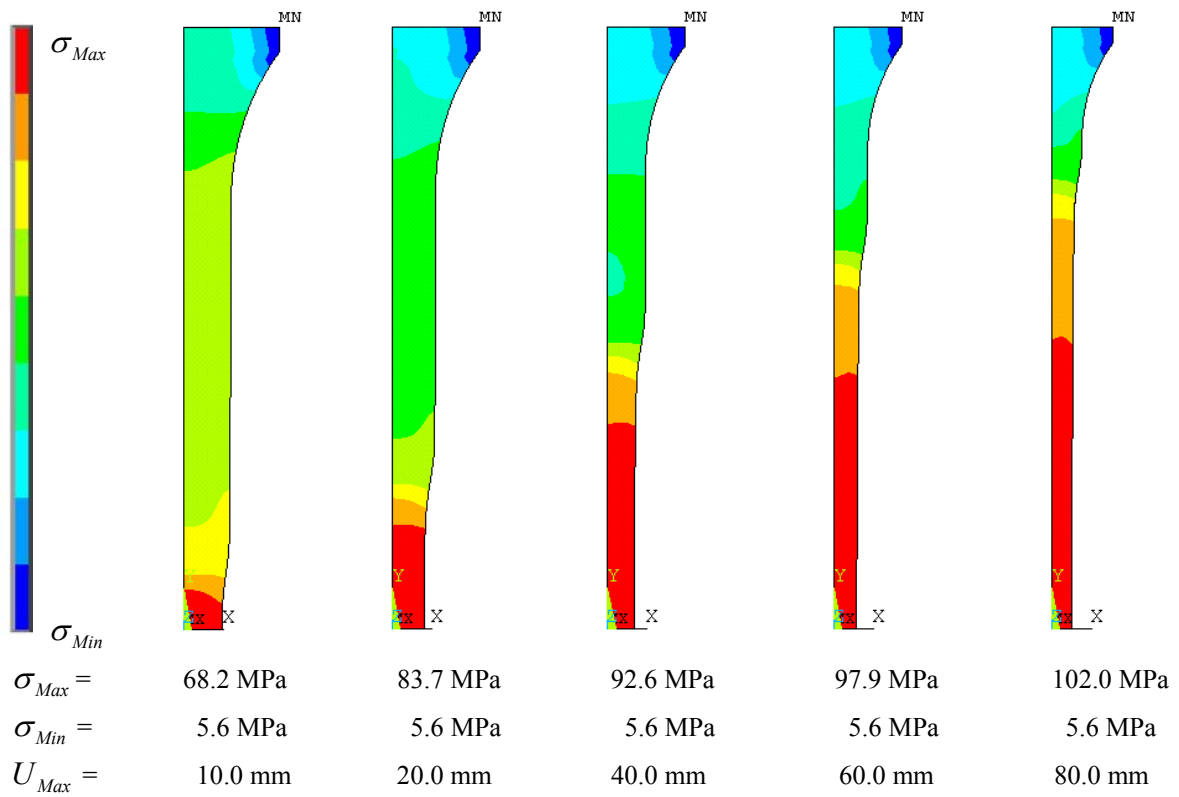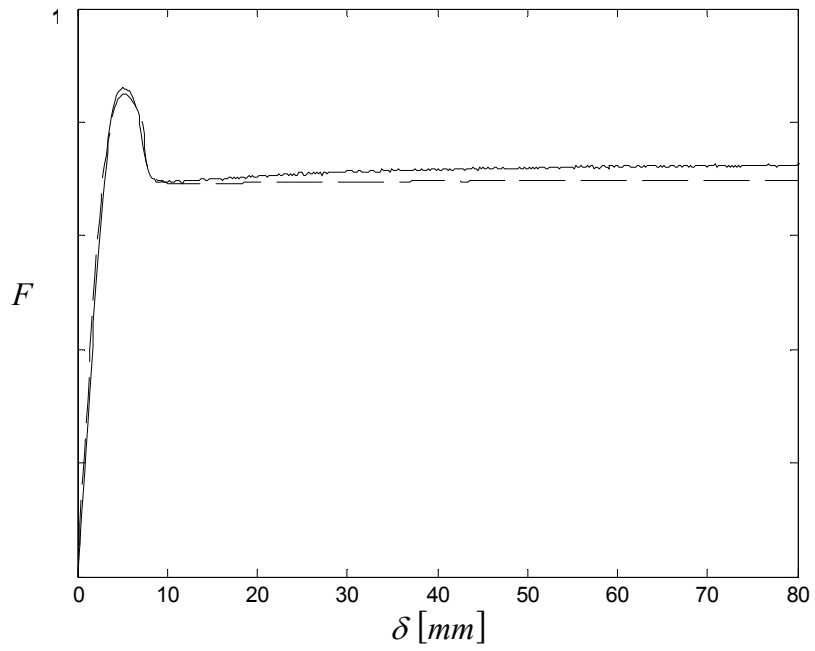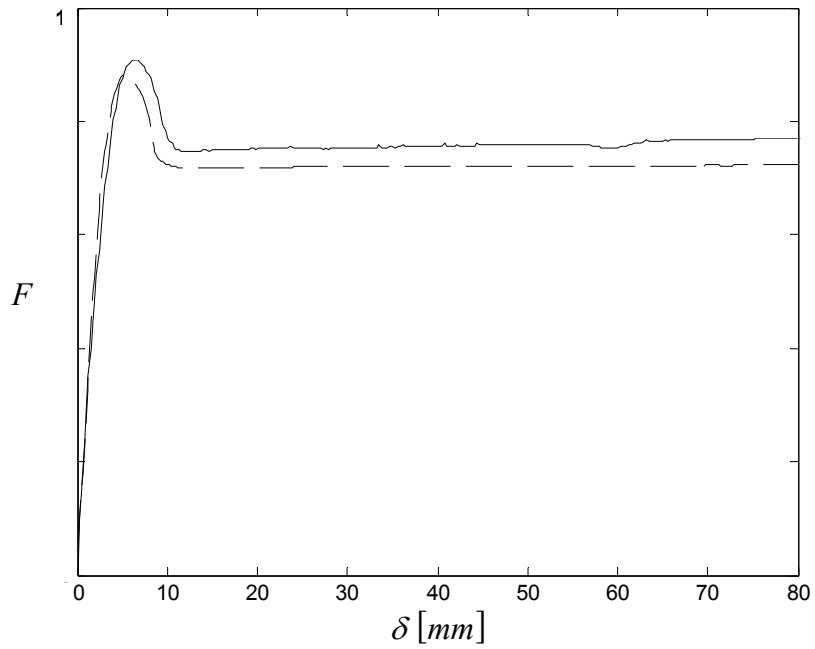
Figure 6.17: A real test (solid line) of PC/ABS at a rate of 6900 mm/min compared with simulation (dashed line).

$\sigma_{Max} =$	63.4 MPa	84.8 MPa	101.0 MPa	111.0 MPa	118.9 MPa
$\sigma_{Min} =$	6.9 MPa	6.5 MPa	6.5 MPa	6.5 MPa	6.5 MPa
$U_{Max} =$	10.0 mm	20.0 mm	40.0 mm	60.0 mm	80.0 mm

Figure 6.18: Von Mises stress of PC/ABS at a rate of 6900 mm/min. U_{Max} refers to global displacement.

Overall the test results show very good agreement with the simulated results, except from the softening behaviour at static condition. It should be pointed out that all tensile tests, show scattering in the results, Figure 6.19 and 6.20, probably due to material imperfections. This spreading partly explains the divergence between the real tests and simulations, throughout.

The slower tensile rates, shows a lower force level before the necking phenomenon initiates, compare Figure 6.9 with Figure 6.17, as mentioned earlier this indicates viscous effects. When comparing the size of the waist area in Figure 6.10, 6.14 and 6.18, it is evident that the strain rate affects the initiating of necking and the size of the waist area enlarges with increasing rate. Exactly what causes this behaviour is hard to describe without further material investigation.
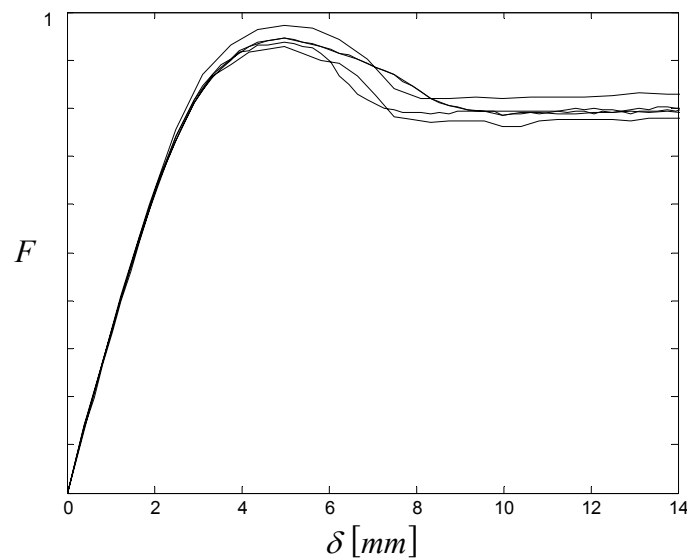

Figure 6.19: The scattering in result. Tensile tests of PC/ABS at a rate of 0.5 mm/min.
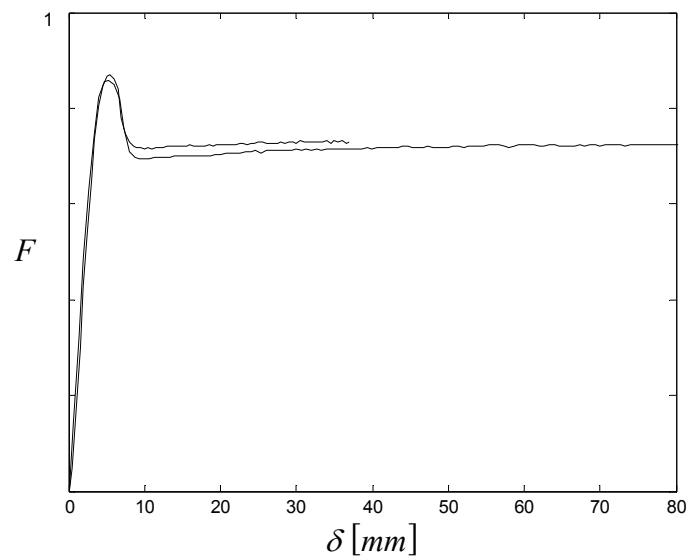

Figure 6.20: The scattering in result. Tensile tests of PC/ABS at a rate of 200 mm/min.

7 Verification of the material model

Tensile tests, with ordinary test specimens are a good way of analysing material behaviour. Unfortunately this test technique can only describe material behaviour in one dimension. Due to this verification tests, so called "specimen with a cylindrical hole", were made to evaluate the whole stress field. This test follows the same test procedure as a normal tensile test but with the difference that now the test specimen has a cylindrical hole at the centre.

7.1 Tensile test of plate with hole

A tensile test was made in the same manner as described in chapter 5.4. This test specimen has the same dimensions according to ISO 527-2/1A, Figure 5.6, with the only difference that it has a 3.2 mm milled cylindrical hole in its centre, Figure 7.2. The addition of the cylindrical hole will describe a multi-axial stress field.

Four different tensile tests were made with increasing strain rates to failure, Figure 7.1.
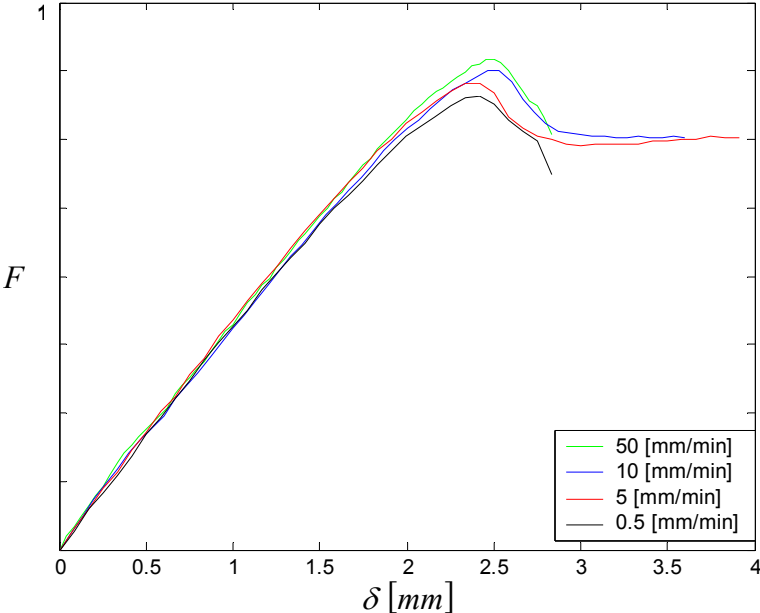

Figure 7.1: Test specimen with cylindrical hole at different rates.

7.2 Simulation of test specimen with hole

7.2.1 Element type and mesh

In the same manner as described in chapter 6.1, a similar tensile test was simulated in ANSYS to verify the results of the tensile test of the specimen with a cylindrical hole, described in 7.1. The mesh of the modelled tensile test specimen is overall identical with the earlier tensile tests described in chapter 6.1, with exception from addition of a cylindrical hole, Figure 7.2. This extra hole gives an increase in number of elements, which are now 2784.
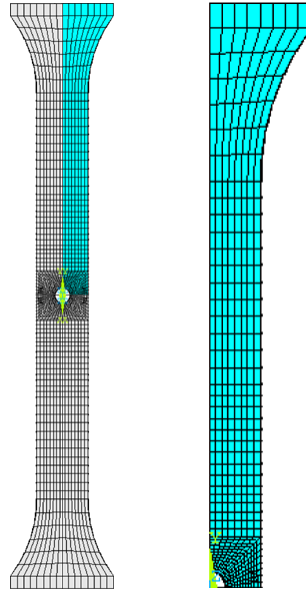

Figure 7.2: Test specimen with a cylindrical hole.

7.2.2 Loads and boundary conditions

Since this test specimen is almost identical to the one earlier described in chapter 6, with exception from the cylindrical hole, the geometrical symmetry can be used. In the same manner as described in chapter 6.1 only a quarter of the test specimen was used for analysis.

Regarding the boundary conditions, these are the same as earlier described, but now with a smaller final displacement U_y at the top, Figure 6.4.

7.2.3 Results

The results from the tensile tests on the specimen with cylindrical hole are compared with the simulation in the same manner as described in chapter 6.4. Since the simulation can not describe the actual failure, one needs to be aware of the limit when failure occurs.
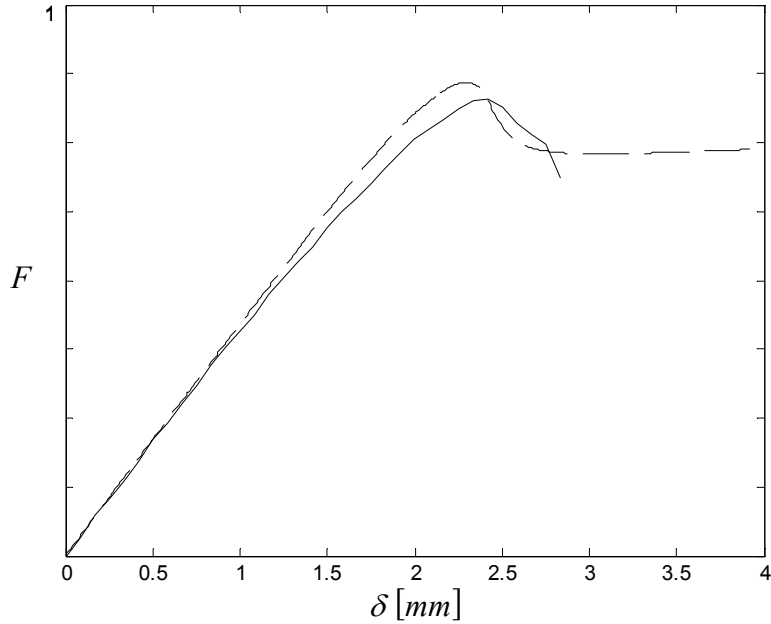

Figure 7.3: A real test of specimen with cylindrical hole (solid line) of PC/ABS at a rate of 0.5 mm/min compared with simulation (dashed line).

$\sigma_{Max} =$	51.2 MPa	105 MPa	119 MPa
$\sigma_{Min} =$	3.78 MPa	3.41 MPa	3.45 MPa
$U_{Max} =$	2.0 mm	3.0 mm	4.0 mm

Figure 7.4: Von Mises stress of PC/ABS at a rate of 0.5 mm/min. U_{Max} refers to global displacement.

Figure 7.5: A real test of specimen with cylindrical hole (solid line) of PC/ABS at a rate of 5 mm/min compared with simulation (dashed line).
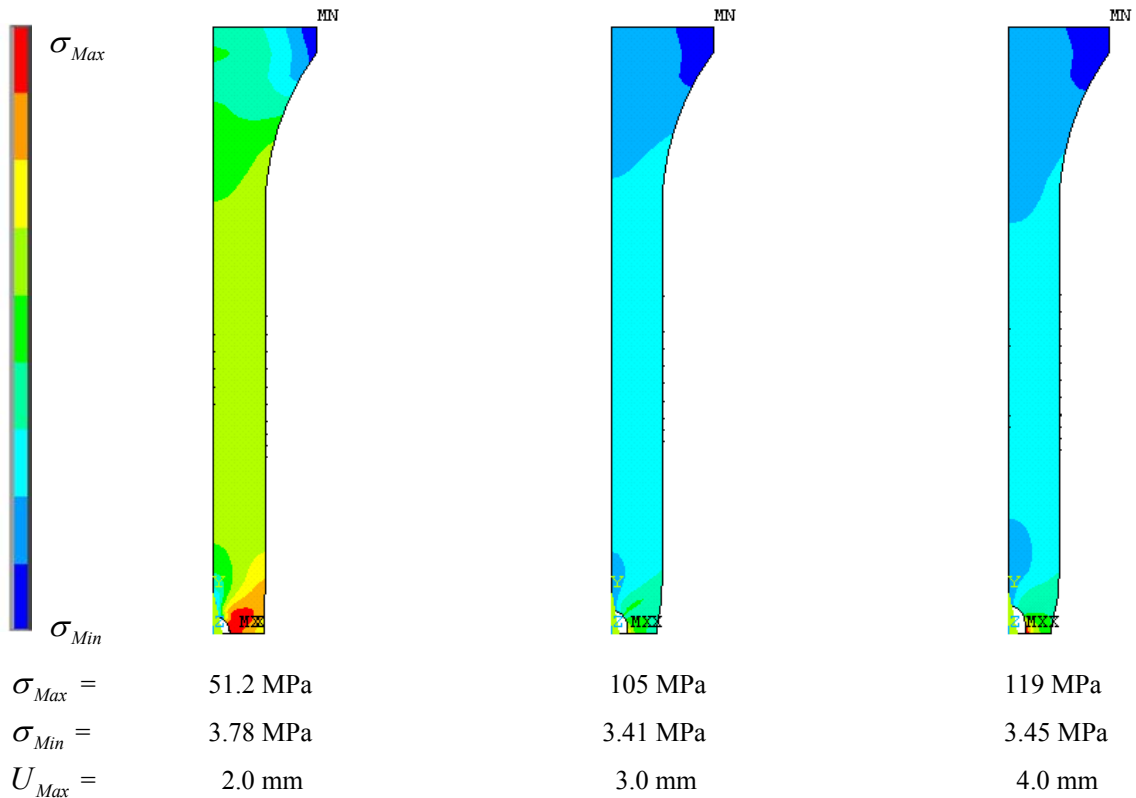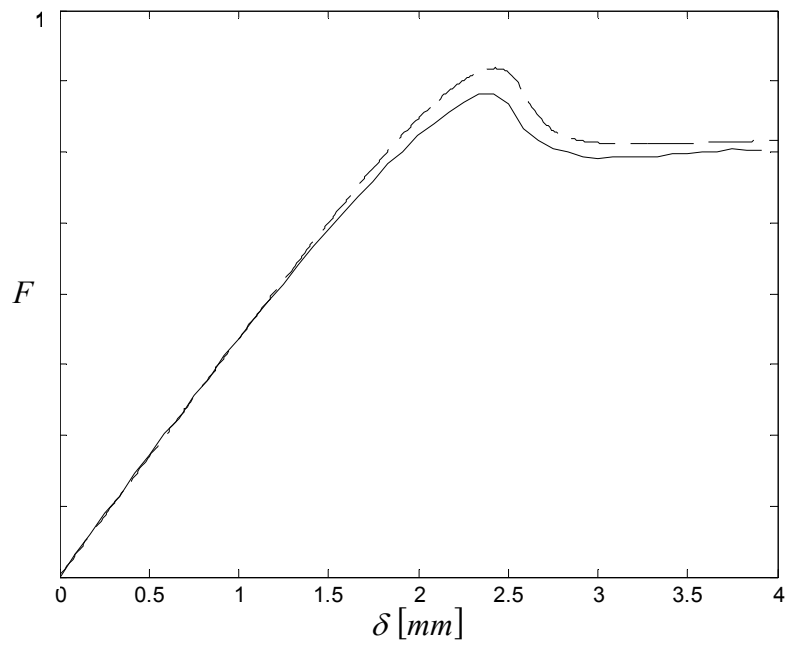

$\sigma_{Max} =$	53.4 MPa	103 MPa	125 MPa
$\sigma_{Min} =$	3.79 MPa	3.58 MPa	3.60 MPa
$U_{Max} =$	2.0 mm	3.0 mm	4.0 mm

Figure 7.6: Von Mises stress of PC/ABS at a rate of 5 mm/min. U_{Max} refers to global displacement.

Figure 7.7: A real test of specimen with cylindrical hole (solid line) of PC/ABS at a rate of 10 mm/min compared with simulation (dashed line).
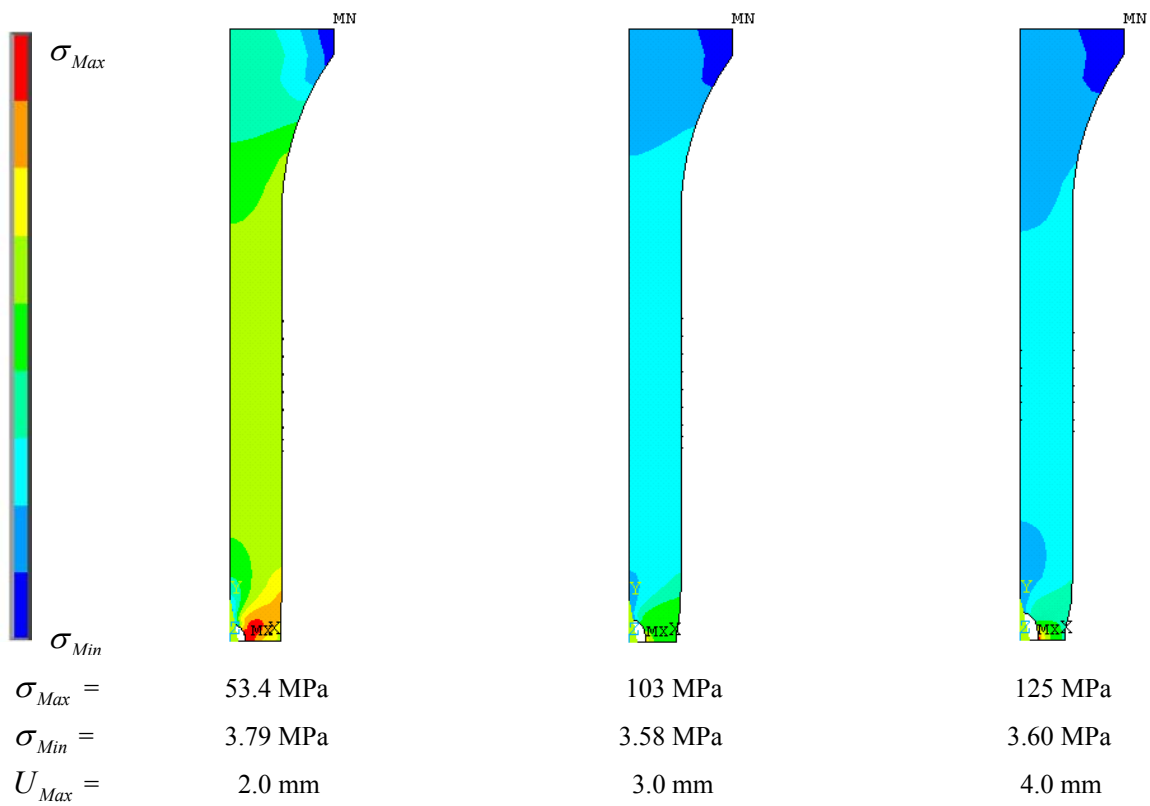

σ_{Max} =	54.3 MPa	102 MPa	127 MPa
σ_{Min} =	3.80 MPa	3.66 MPa	3.66 MPa
U_{Max} =	2.0 mm	3.0 mm	4.0 mm

Figure 7.8: Von Mises stress of PC/ABS at a rate of 10 mm/min. U_{Max} refers to global displacement.

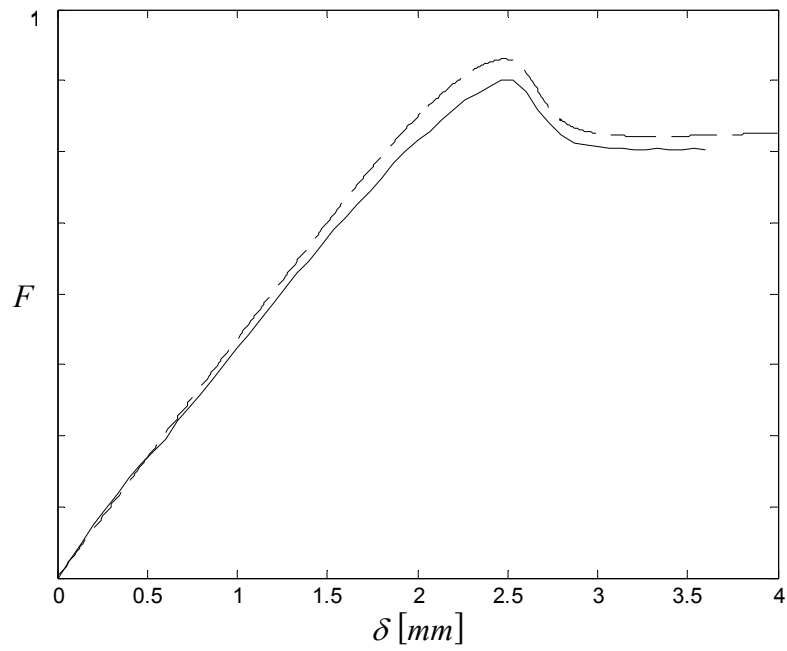**Figure 7.9:** A real test of specimen with cylindrical hole (solid line) of PC/ABS at a rate of 50 mm/min compared with simulation (dashed line).
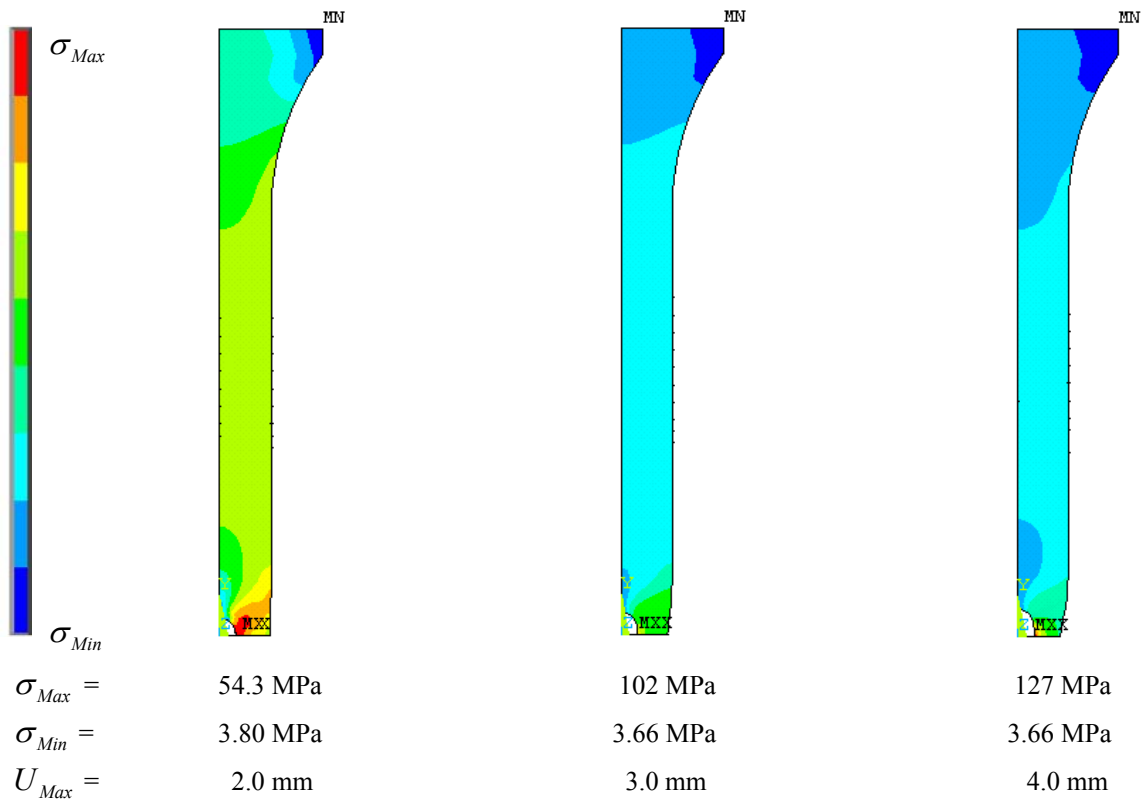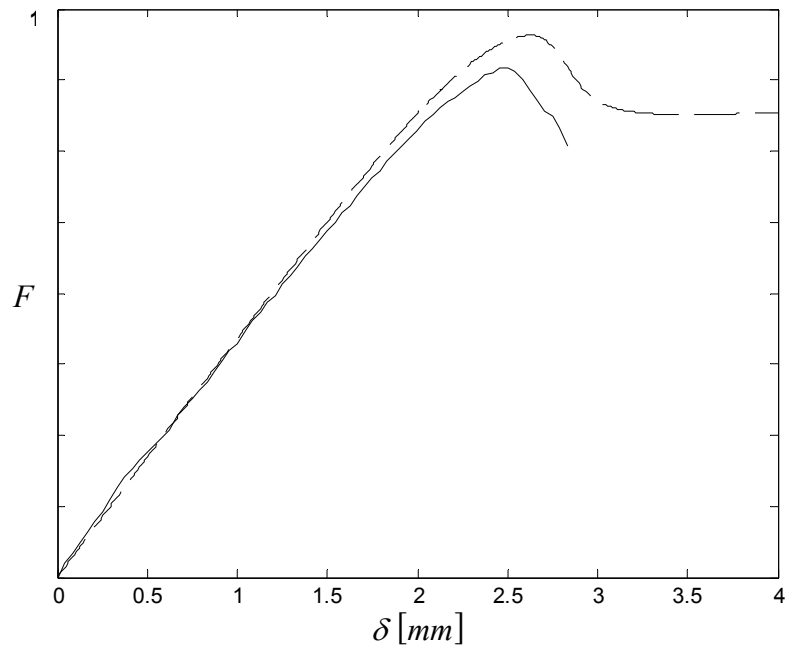

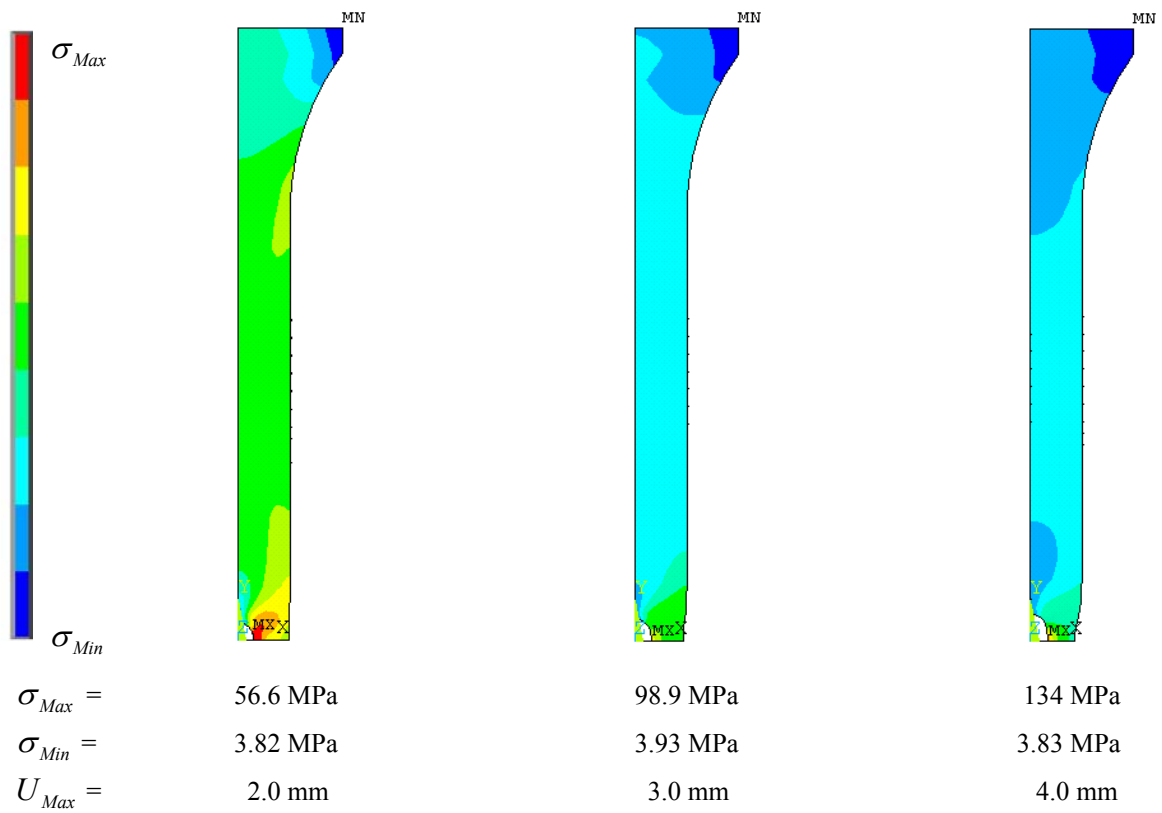| σ_{Max} = | 56.6 MPa | 98.9 MPa | 134 MPa |
| σ_{Min} = | 3.82 MPa | 3.93 MPa | 3.83 MPa |
| U_{Max} = | 2.0 mm | 3.0 mm | 4.0 mm |

Figure 7.10: Von Mises stress of PC/ABS at a rate of 50 mm/min. U_{Max} refers to global displacement.

53

The overall test results show very good agreement with the simulated results, Figure 7.3, 7.5, 7.7 and 7.9. Still there is a spreading in result due to material imperfections, which will affect the results of the test comparison overall.

In the same way as in chapter 6, the lower tensile rates, show a lower force level before softening initiates, Figure 7.3, 7.5, 7.7 and 7.9. It is noticeable that the strain rate influencing the initiating of softening and the size of the waist area enlarges with increasing rate, Figure 7.4, 7.6, 7.8 and 7.10. Overall the Perzyna model seems to describe the whole stress field satisfactorily.

8 Conclusions

The investigated plastic, PC/ABS, shows a highly viscous behaviour, i.e. highly rate-dependent. In large strain applications for materials where the cross section area changes, it is important to use input data in terms of true stress and true strain, to maintain the accuracy. Use of engineering data of PC/ABS in simulation programs makes the results less reliable, particularly after necking has been initiated.

Data of true stress and true strain is not available either in the literature or from the material supplier. This data can be obtained by comparing simulations of tensile tests with real tensile tests.

The only useful material models in ANSYS for large strain rates, is the visco-plastic model namely, the Perzyna model.
This model requires identification of the two parameters γ and m to describe the visco-plastic behaviour. Due to the request for secrecy these parameters can not be published.

The Perzyna model describes the softening behaviour well and global strains up to 80 % at analyzed strain rates. Overall the test results show satisfying agreement with the simulated results, with the only exception for static condition, where the agreement between real tests and simulations were not totally satisfying in the softening region. This drawback arises from the Perzyna model approaching isotropic hardening plasticity at slow strain rates. Isotropic hardening plasticity is not able to describe this softening in a satisfying manner.

A uniaxial tensile test can only describe material behaviour in one dimension. Due to that, a verification tensile test using a specimen with a cylindrical hole was made. This test describes the whole stress field. The results are satisfying in all analyzed strain rates for Perzyna model.

9 References

[1] Aleksey, D. D. (1999), *A Constitutive Model in Viscoelastoplasticity of Glassy Polymers*, Polymer, Vol. 40, pp. 3711-3727.

[2] Anand L. and Lush A. M. and Weber G. G. and Zavaliangos A. (1990), *An Objective Time-integration Procedure for Isotropic Rate-independent and Rate-dependent Elastic-plastic Constitutive Equations*, International Journal of Plasticity, Vol. 6, pp. 701-744.

[3] ANSYS, Inc (2000), *Structural Analysis Guide*, ANSYS Release 5.7, SAS IP, Inc, USA.

[4] Arruda, E. M. and Boyce, M. C. (1990), *An Experimental and Analytical Investigation of the Large Strain Compressive and Tensile Response of Glassy Polymers*, Polymer Engineering and Science, Vol. 30, No. 20, pp. 1288-1298.

[5] Arruda, E. M. and Boyce, M. C. and Jayachandran, R. (1994), *The Large Strain Compression, Tension and Simple Shear of Polycarbonate*, Polymer Engineering and Science, Vol. 34, No 9, pp. 716-725.

[6] Belytschko, T. and Liu, K. W. and Moran, B. (2001), *Nonlinear Finite Elements for Continua and Structures*, John Wiley and Sons, Ltd, Baffins Lane, Chichester, ISBN 0-471-98773-5.

[7] Bonniers Stora Lexikon på CD (2000), Bonnier Lexikon AB.

[8] Boyce, M. C. and Arruda, E. M. (1990), *An experimental and analytical investigation of the large strain compressive and tensile response of glassy polymers*, Polymer Engineering and Science, Vol. 30, No 20, pp. 1288-98.

[9] Brown and Bubeck and Buckley and Kraemer, *Modes of deformation in rubber modified thermoplastics during tensile impact*, Journal of Material Science.

[10] Campus 4.1 (1999), GE Plastics Europe.

[11] Chandrakant, S. D. and Hema, J. S. (1984), *Constitutive Laws for Engineering Materials with Emphasis on Geologic Materials*, Prentice-Hall, Inc., Englewood Cliffs, New Jersey.

[12] Dally, J. W. and Mulc, A. (1973), *Polycarbonate as a Model Material for Three-Dimensional Photoplasticity*, Journal of Applied Mechanics, Vol. 40, No. 2, pp. 600-605.

[13] Hadjiiossiph, C. and Theocaris, P. S. (1979), *Strain-Analysis of Neck Formation and Propagation in Glassy Polymers*, Engineering Fracture Mechanics, Vol. 12, No. 2, pp. 241-252.

[14] Hughes, T. J. R. and Simo, J. C. (2000), *Compuantional Inelasticity*, ISBN 0-387-97520-9, Springer-verlag New York, Inc.

[15] Klason, C. and Kubát, J. (2001), *Plaster Materialval och materialdata*, Författarna och Industrilitteratur AB, Utgåva 5.

[16] Lundgren, E. (2003), Lectures notes, Division of Mechanics, University of Lund.

[17] Miller, L. C. and Nimmer, R. P. (1984), *Neck Propagation in Tensile Tests: A Study Using Rate-Independent, Strain Hardening Plasticity*, Journal of Applied Mechanics, Vol. 51, pp. 759-765.

[18] Ottosen, S. N. and Ristinmaa, M. (1996), *Large strain plasticity and thermodynamics*, Division of Solid Mechanics, University of Lund.

[19] Ottosen, S. N. and Ristinmaa, M. (1999), *The Mechanics of Constitutive Modelling*, volume 1, Division of Solid Mechanics, University of Lund.

[20] Owen, D. R. J. and Peric, D. (1992), *A Model for Large Deformations of Elasto-Viscoplastic Solids at Finite Strains: Computational Issues, Finite Inelastic Deformations: Theory and Applications*, Springer-Verlag, Berlin.

[21] Sony Ericsson Mobile Communications AB (2004-03-29), About Us, http://www.sonyericsson.com/uk/

[22] Vincent, P. I. (1960), *The Necking and Cold-Drawing of Rigid Plastics*, Polymer, Vol. 1, No. 7.